

# Cortical Ripples during NREM Sleep and Waking in Humans

 Charles W. Dickey,<sup>1,2</sup> Ilya A. Verzhbinsky,<sup>1,2</sup> Xi Jiang,<sup>1</sup> Burke Q. Rosen,<sup>1</sup> Sophie Kajfez,<sup>3</sup> Emad N. Eskandar,<sup>4</sup> Jorge Gonzalez-Martinez,<sup>5</sup>  Sydney S. Cash,<sup>6</sup> and Eric Halgren<sup>3,7</sup>

<sup>1</sup>Neurosciences Graduate Program, University of California San Diego, La Jolla, California 92093, <sup>2</sup>Medical Scientist Training Program, University of California San Diego, La Jolla, California 92093, <sup>3</sup>Department of Radiology, University of California San Diego, La Jolla, California 92093, <sup>4</sup>Department of Neurological Surgery, Montefiore Medical Center, Albert Einstein College of Medicine, Bronx, New York 10461, <sup>5</sup>Department of Neurological Surgery, University of Pittsburgh, Pittsburgh, Pennsylvania 15260, <sup>6</sup>Department of Neurology, Massachusetts General Hospital, Harvard Medical School, Boston, Massachusetts 02114, and <sup>7</sup>Department of Neurosciences, University of California San Diego, La Jolla, California 92093

Hippocampal ripples index the reconstruction of spatiotemporal neuronal firing patterns essential for the consolidation of memories in the cortex during non-rapid eye movement sleep (NREM). Recently, cortical ripples in humans have been shown to enfold the replay of neuron firing patterns during cued recall. Here, using intracranial recordings from 18 patients (12 female), we show that cortical ripples also occur during NREM in humans, with similar density, oscillation frequency ( $\sim 90$  Hz), duration, and amplitude to waking. Ripples occurred in all cortical regions with similar characteristics, unrelated to putative hippocampal connectivity, and were less dense and robust in higher association areas. Putative pyramidal and interneuron spiking phase-locked to cortical ripples during NREM, with phase delays consistent with ripple generation through pyramidal–interneuron feedback. Cortical ripples were smaller in amplitude than hippocampal ripples but were similar in density, frequency, and duration. Cortical ripples during NREM typically occurred just before the upstate peak, often during spindles. Upstates and spindles have previously been associated with memory consolidation, and we found that cortical ripples grouped cofiring between units within the window of spike timing-dependent plasticity. Thus, human NREM cortical ripples are as follows: ubiquitous and stereotyped with a tightly focused oscillation frequency; similar to hippocampal ripples; associated with upstates and spindles; and associated with unit cofiring. These properties are consistent with cortical ripples possibly contributing to memory consolidation and other functions during NREM in humans.

**Key words:** cortex; hippocampus; humans; ripples; sleep; waking

## Significance Statement

In rodents, hippocampal ripples organize replay during sleep to promote memory consolidation in the cortex, where ripples also occur. However, evidence for cortical ripples in human sleep is limited, and their anatomic distribution and physiological properties are unexplored. Here, using human intracranial recordings, we demonstrate that ripples occur throughout the cortex during waking and sleep with highly stereotyped characteristics. During sleep, cortical ripples tend to occur during spindles on the down-to-upstate transition, and thus participate in a sequence of sleep waves that is important for consolidation. Furthermore, cortical ripples organize single-unit spiking with timing optimal to facilitate plasticity. Therefore, cortical ripples in humans possess essential physiological properties to support memory and other cognitive functions.

Received Apr. 14, 2022; revised July 19, 2022; accepted July 22, 2022.

Author contributions: C.W.D. and E.H. designed research; C.W.D., I.A.V., E.N.E., J.G.-M., S.S.C., and E.H. performed research; C.W.D., I.A.V., X.J., B.Q.R., and S.K. contributed unpublished reagents/analytic tools; C.W.D., I.A.V., and X.J. analyzed data; C.W.D. and E.H. wrote the first draft of the paper; C.W.D. and E.H. edited the paper; C.W.D. and E.H. wrote the paper.

This work was supported by National Institute of Mental Health 1R01MH117155-01 and T32 MH020002, and Office of Naval Research Multidisciplinary University Research Initiative N00014-16-1-2829. We thank Adam Niese, Christine Smith, Christopher Gonzalez, Daniel Cleary, Eran Mukamel, Erik Kaestner, Jacob Garrett, Maxim Bazhenov, Terrence Sejnowski, and Zarek Siegel for support.

The authors declare no competing financial interests.

Correspondence should be addressed to Eric Halgren at ehalgren@health.ucsd.edu or Charles W. Dickey at cddickey@health.ucsd.edu.

<https://doi.org/10.1523/JNEUROSCI.0742-22.2022>

Copyright © 2022 the authors

## Introduction

Hippocampal ripples have been extensively studied in rodents during non-rapid eye movement sleep (NREM), when they mark the replay of events from the prior waking period, and are critical for memory consolidation in the cortex (Wilson and McNaughton, 1994; Girardeau et al., 2009; Ego-Stengel and Wilson, 2010; Buzsáki, 2015; Maingret et al., 2016). They are associated with cortical replay (Ji and Wilson, 2007; Peyrache et al., 2009; L. A. Johnson et al., 2010), and with cortical sleep waves (spindles, downstates, upstates) (Siapas and Wilson, 1998), a relationship crucial for consolidation

**Table 1.** SEEG patient demographics and data characteristics<sup>a</sup>

Patient	Age (yr)	Sex	Handedness	No. of cortical channels	No. of hippocampal channels	NREM duration (h)	Waking duration (h)	$\delta$ NREM/ $\delta$ waking <sup>b</sup>
S1	20	M	R	18 (L)	1 (L)	6.1	49.8	3.98
S2	58	F	R	22 (L)	2 (L)	23.7	23.8	2.35
S3	42	M	L	16 (3 L)	3 (2 L)	11.4	19.3	3.39
S4	18	F	L	15 (R)	2 (R)	2.7	2.2	3.02
S5	20	F	R	18 (7 L)	2 (R)	5.6	19.3	2.93
S6	22	M	LR	17 (L)	1 (L)	6.3	59.9	5.45
S7	30	F	R	13 (2 L)	1 (R)	20.5	76.7	4.46
S8	43	F	R	12 (L)	2 (L)	8.1	32.6	5.43
S9	16	M	R	16 (4 L)	1 (R)	16.3	4.8	2.50
S10	32	F	R	29 (3 L)	3 (1 L)	11.2	27.6	3.11
S11	21	F	L	8 (4 L)	3 (2 L)	16.0	52.6	3.04
S12	21	F	R	14 (13 L)	1 (L)	26.2	37.2	2.92
S13	29	F	R	15 (6 L)	2 (1 L)	8.6	24.6	3.75
S14	41	F	R	18 (R)	1 (R)	11.9	63.3	4.20
S15	24	M	R	21 (9 L)	1 (L)	11.8	11.6	3.27
S16	31	F	R	15 (7 L)	1 (L)	28.1	39.4	2.55
S17	21	M	R	6 (L)	1 (L)	11.3	18.9	1.41

<sup>a</sup>Channels are the bipolar derivations included in the analyses.<sup>b</sup> $\delta$  NREM/ $\delta$  waking reports the ratio of the mean of the  $\delta$  (0.5–2 Hz) analytic amplitude means across cortical channels during the NREM versus waking epochs analyzed.

(Latchoumane et al., 2017). Rat hippocampal ripples comprise a  $\sim$ 140 Hz oscillation riding on the peak of a  $\sim$ 70 ms duration sharp-wave, followed by a slower local potential (Buzsáki, 2015). Human hippocampal sharp-wave-ripples also occur during NREM with similar temporal relationships to cortical spindles and down-to-upstates, and similar hippocampal topography, but with a median frequency of 80–90 Hz (Staresina et al., 2015; Jiang et al., 2019a,b,c).

Recently, ripples were found in rat association cortex but not primary sensory or motor cortices during sleep, with increased coupling to hippocampal ripples in sleep following learning (Khodagholy et al., 2017). An earlier study reported ripples in waking and sleeping cat cortex, especially during NREM (Grenier et al., 2001). In humans, cortical ripples during waking were more frequently found in lateral temporal than rolandic cortex, and coupled to parahippocampal gyrus ripples more often before correct paired-associates recall (Vaz et al., 2019). Lateral temporal units fired in-phase with the local waking ripples in patterns previously observed during learning (Vaz et al., 2020). Waking hippocampal ripples were also associated with cortical activity patterns selective for faces and buildings during free recall (Norman et al., 2019). Evidence for cortical ripples during NREM in humans is limited, but a previous study indicated that they may be suppressed during, and increased following, the cortical downstate (von Ellenrieder et al., 2016).

Thus, there is an emerging appreciation that, in humans and rodents, hippocampal and cortical ripples play an important role in memory during both sleep and waking. However, many fundamental questions remain unresolved. The basic characteristics of ripples have not been compared between the cortex and hippocampus, or between sleep and waking, so it is unclear how ripples may differ between their putative roles of supporting consolidation versus recall, or indeed if they represent the same phenomenon. Knowledge of the distribution of ripples across different cortical areas during waking is limited and during sleep is essentially absent. The relations between cortical ripples and local sleep spindles, downstates, and upstates have not been determined. Such relations could support a role of cortical ripples in consolidation, as would increased cofiring between neurons within the window of spike timing-dependent plasticity (STDP). Furthermore, the relationships of human cortical

pyramidal and inhibitory cell-firing to ripples and to each other, important for understanding ripple generation, have not been determined.

Here, using intracranial stereoelectroencephalography (SEEG) recordings, we show that cortical ripples are generated during NREM in humans, and we provide the first comprehensive characterization of cortical ripples. Ripples with a stereotyped, tightly focal oscillation frequency of  $\sim$ 90 Hz and duration of  $\sim$ 70 ms were ubiquitous throughout the cortex during waking and NREM, although slightly less dense and robust in association areas, and with no relationship to putative hippocampal connectivity. We found that cortical ripples are similar to hippocampal in oscillation frequency, density, and duration. Cortical ripples in NREM coupled strongly to down-to-upstates, and less often to spindles, consistent with a possible role in memory replay. Using single-unit recordings from a cortical microarray, we identify the probable generating circuits of cortical ripples and show that units cofire during ripples at short delays that are optimal for STDP. Thus, human cortical ripples during NREM have the necessary physiological properties to facilitate replay-guided plasticity. However, the ubiquity and stereotypy of human ripples across structures and states are also consistent with a more general functional role.

## Materials and Methods

**Patient selection.** Data from a total of 18 patients (12 female,  $30.0 \pm 12.2$  years old) with pharmaco-resistant epilepsy undergoing intracranial recording for seizure onset localization preceding surgical treatment were included in this study (Table 1). Patients whose SEEG recordings were analyzed were only included in the study if they had no prior brain surgery; background EEG (with the exception of epileptiform transients) in the normal range; and electrodes implanted in what was eventually found to be nonlesional, nonepileptogenic cortex, as well as nonlesional, nonepileptogenic hippocampus (such areas were suspected to be part of the focus before implantation, or were necessary to pass through to reach suspected epileptogenic areas).

Furthermore, 1 of these patients (51-year-old right-handed female) was also implanted with an intracranial microelectrode (Utah Array) into tissue that was suspected based on presurgical evaluation to be included within the region of the therapeutic resection. The implantation of the array did not affect clinical monitoring. It was later resected to gain access to the surgical focus beneath, the electrode was determined

not to be implanted in an epileptogenic zone, and no seizures originated from the region of the array.

Patients were excluded from the study if they had prior brain surgery or did not have nonlesioned hippocampal and cortical channels that were not involved in the early stage of the seizure discharge and did not have frequent interictal activity or abnormal local field potentials (LFPs). Utah Array patients were only included in the study if they had at least 20 pyramidal cells (PYs) and 20 interneurons (INs). Based on these criteria, 18 patients were included in this study of 84. All patients gave fully informed written consent for their data to be used for research as monitored by the local Institutional Review Boards at Cleveland Clinic and Partners HealthCare (including Massachusetts General Hospital).

**Intracranial recordings.** Patients were implanted with intracranial electrodes for ~7 d with continuous recordings for seizure onset localization. SEEG electrode implantation and targeting were made for purely clinical purposes. SEEG recordings were collected with a Nihon Kohden JE-120 amplifier at 1000 Hz sampling (Patients S1–S17). Standard clinical electrodes were 0.8 mm diameter, with 10–16 contacts of length 2 mm at 3.5–5 mm pitch (~150 contacts/patient).

Microelectrode recordings from 1 patient implanted with a Utah Array were also analyzed (200 min of NREM). The Utah Array is a 10 × 10 microelectrode array with corners omitted and 400 μm contact pitch (Waziri et al., 2009; Keller et al., 2010; Fernández et al., 2014). Each silicon probe is 1 mm long with a base of 35–75 μm that tapers to 3–5 μm. The probes are insulated, except for the platinum-coated tip. Data were acquired at 30 kHz (Blackrock Microsystems) with a 0.3–7.5 kHz bandpass. Data were recorded with respect to a distant reference wire.

**Electrophysiology preprocessing.** Offline data preprocessing was performed in MATLAB 2019b, and LFPs were inspected visually using the FieldTrip toolbox (Oostenveld et al., 2011). SEEG data were downsampled to 1000 Hz with anti-aliasing and 60 Hz notch filtered (zero-phase) with 60 Hz harmonics up to 480 Hz. Transcortical contact pairs were identified using both anatomic location (using the preoperative MRI aligned to the postoperative CT), and physiological properties (high amplitude, coherence, and inversion of spontaneous activity between contacts), and selected such that no 2 pairs shared a contact. All SEEG analyses were performed using bipolar derivations between adjacent contacts in cortical or hippocampal gray matter to ensure that activity was locally generated (Mak-McCully et al., 2015).

**Channel selection.** Channels were excluded from analysis if they were in lesioned tissue, involved in the early stages of the seizure discharge, or had frequent interictal activity or abnormal LFPs. From the total 2129 bipolar channels (1202 left hemisphere) of the 17 SEEG patients (S1–S17), 28 hippocampal (16 left hemisphere) and 273 transcortical (133 left hemisphere) bipolar channels were selected for the analyses (Table 1). Most channels were rejected because they did not constitute a transcortical pair as described above. First, most bipolar pairs were in the white matter, and thus did not record focal cortical activity. In addition, many channels were rejected for the related criterion that one of the contacts was in common with another bipolar pair that was already selected. This was done because a common contact means that the two bipolar pairs would not provide independent measurements. Polarity was corrected for individual bipolar channels such that downstates were negative and upstates were positive. This was accomplished by ensuring that negative peaks during NREM were associated with decreased and positive peaks were associated with increased mean  $\pm 100$  ms 70–190 Hz analytic amplitude, an index of cell-firing that is strongly modulated by downstates and upstates (Csersca et al., 2010).

**Electrode localization.** Cortical surfaces were reconstructed from the preoperative whole-head T1-weighted structural MR volume using the standard FreeSurfer recon-all pipeline (Fischl, 2012). Atlas-based automated parcellation (Fischl et al., 2004) was used to assign anatomic labels to regions of the cortical surface in the Destrieux atlas (Destrieux et al., 2010). In addition, automated segmentation was used to assign anatomic labels to each voxel of the MR volume, including identifying voxels containing hippocampal subfields (Iglesias et al., 2015). In order to localize the SEEG contacts, the postimplant CT volume was registered to the MR volume, in standardized 1 mm isotropic FreeSurfer space, using the general registration module (H. Johnson et al., 2007) in 3D Slicer (Fedorov

**Table 2. Relationships between cortical regions reported and Desikan parcels<sup>a</sup>**

Cortical region	Desikan parcels
Orbitofrontal	Frontal pole, lateral orbitofrontal, medial orbitofrontal, pars orbitalis
Prefrontal	Caudal middle frontal, pars opercularis, pars triangularis, rostral middle frontal, superior frontal
Rolandic	Paracentral, postcentral, precentral
Parietal	Inferior parietal, superior parietal, supramarginal, precuneus
Occipital	Cuneus, pericalcarine, lateral occipital
Superior temporal/insula	Insula, superior temporal, transverse temporal
Lateral temporal	Banks of superior temporal gyrus, inferior temporal, middle temporal
Ventral temporal	Entorhinal, fusiform, lingual, parahippocampal, temporal pole, isthmus cingulate
Cingulate	Caudal anterior cingulate, rostral anterior cingulate, posterior cingulate

<sup>a</sup>First column lists the cortical regions described in this study, which are derived from an amalgamation of the cortical parcels from Desikan et al. (2006) listed in the second column.

et al., 2012). The position of each SEEG contact, in FreeSurfer coordinates, was then determined by manually annotating the centroids of the electrode contact visualized in the coregistered CT volume. Each transcortical contact pair was assigned an anatomic parcel from the atlas above by ascertaining the parcel identities of the surface vertex closest to the contact pair midpoint. Subcortical contacts were assigned an anatomic label corresponding to the plurality of voxel segmentation labels within a 2 voxel radius. Transcortical contact pair locations were registered to the fsaverage template brain for visualization by spherical morphing (Fischl et al., 1999). To plot values on a template brain, channel means were averaged for each cortical region, using amalgamations of the parcels from Desikan et al. (2006) (Table 2), with the two hemispheres combined, and then morphed onto a left hemisphere ico5 fsaverage template. White-matter streamline distances between channels were computed using the 360 parcels of the HCP-MMP1.0 atlas (Glasser et al., 2016), as determined by probabilistic diffusion MRI tractography (Behrens et al., 2007), and are population averages from Rosen and Halgren (2021). When two channels were in the same HCP parcel, the distance was considered to be 0.

**Time-frequency analyses.** Average time-frequency plots of the ripple event-related spectral power were generated from the broadband LFP using EEGLAB (Delorme and Makeig, 2004). Event-related spectral power was calculated from 1 Hz to the Nyquist frequency (500 Hz) with 1 Hz resolution with ripple centers at  $t = 0$  by computing and averaging fast Fourier transforms with Hanning window tapering. Each 1 Hz bin of the time-frequency matrix was normalized with respect to the mean power at  $-2000$  to  $-1500$  ms and masked with two-tailed bootstrapped significance ( $N = 200$ ) with false discovery rate (FDR) correction and  $\alpha = 0.05$  using  $-2000$  to  $-1500$  ms as baseline. Grand average time-frequency plots were generated by averaging the average time-frequency plots of all channels for a given region (i.e., neocortex or hippocampus) and state (i.e., NREM or waking).

**Sleep and waking epoch selection.** Epochs included in the study did not fall within at least 1 h of a seizure and were not contaminated with frequent interictal spikes (IISs) or artifacts. NREM periods were selected from continuous overnight recordings where the  $\delta$  (0.5–2 Hz) analytic amplitude from the cortical channels was persistently increased (Table 1). Sleep epochs were confirmed by visual inspection to have normal appearing downstates, upstates, and spindles. Downstates, upstates, and spindles were also automatically detected, and quantification of these events showed they had the densities, amplitudes, and frequencies that are characteristic of NREM (see details in Detection of downstates, upstates, and sleep spindles). Waking periods were selected from continuous daytime recordings that had persistently low cortical  $\delta$  as well as high cortical  $\alpha$  (8–12 Hz),  $\beta$  (20–40 Hz), and high  $\gamma$  (70–190 Hz) analytic amplitudes. When the data included EOG ( $N = 15/17$  SEEG patients), waking periods also required that the 0.5–40 Hz analytic amplitude of the EOG trace was

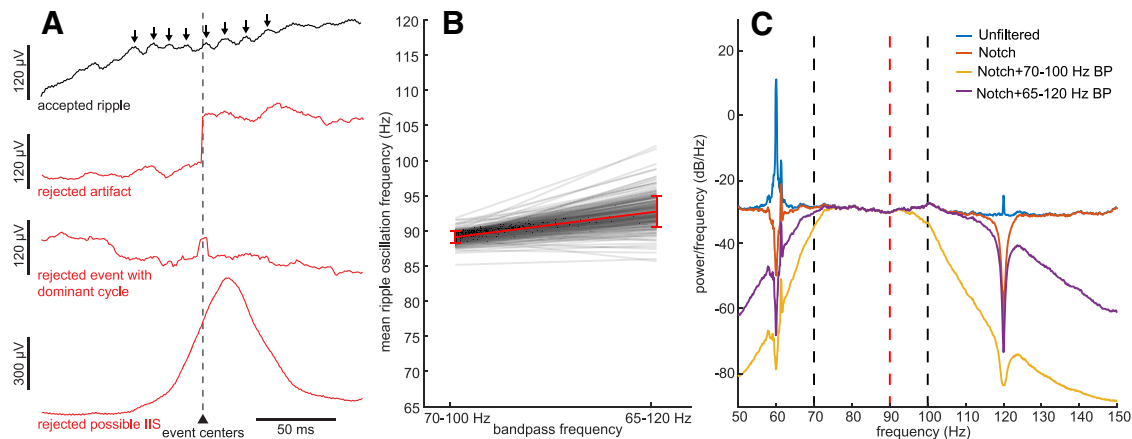


**Figure 1.** Ripple detection and event rejection. **A**, Broadband LFP single sweeps show events that exceeded amplitude thresholds and were accepted for or rejected from the analyses. Traces represent an example accepted ripple, with black arrows indicating multiple 70–100 Hz oscillation cycles, a rejected artifact, a rejected event with a single dominant cycle, and a rejected possible IIS. Putative ripples within  $\pm 500$  ms of possible IIS detected on the same channel, as well as putative ripples coinciding with the sharp component of possible IIS on any cortical or hippocampal channel were rejected. **B**, Mean  $\pm$  SD NREM ripple oscillation frequency (red line) across channels ( $N = 273$ ; black lines) from all SEEG patients (S1–S17) is highly similar when using either a 70–100 Hz bandpass (mean  $\pm$  SD =  $89.1 \pm 0.8$  Hz) or a 65–120 Hz bandpass ( $92.7 \pm 2.2$  Hz). **C**, Average power spectral density of unfiltered, notched (60 Hz and harmonics), notched and 70–100 Hz bandpassed, as well as notched and 65–120 Hz bandpassed ( $N = 1000$  randomly selected 27-s-long epochs over 450 min of recording from Patient S2). Dashed black lines indicate 70–100 Hz bandpass used for the main analyses in this study. Dashed red line indicates 90 Hz, the approximate average ripple frequency across states, structures, and filter settings.

increased. Waking epochs were required to be separated from periods of increased  $\delta$  analytic amplitude by at least 30 min.

**Ripple detection.** The median center frequency of hippocampal ripples in nine studies was  $\sim 85$  Hz in humans (Bragin et al., 1999; Staba et al., 2004; Clemens et al., 2007; Axmacher et al., 2008; Le Van Quyen et al., 2008; Staresina et al., 2015; Jiang et al., 2019b; Norman et al., 2019; Vaz et al., 2019), whereas in rodents, sharp-wave-ripple frequency is  $\sim 120$ – $140$  Hz (Buzsáki, 2015). In humans, putative 90 Hz hippocampal ripples have the same characteristic relation to sharp-waves, intrahippocampal localization, modulation by sleep stage, and relation to cortical sleep waves as in rodents, and occur in hippocampi that have no signs of epileptic involvement. Furthermore, in rodent hippocampus, the distinction between higher frequency  $\gamma$  bursts and ripples is not always sharp, leading to the suggestion that for simplicity they both be referred to as “ripples” (Stark et al., 2014), which we follow here.

Ripple detection was performed in the same way for all structures and states and was based on a previously described hippocampal ripple detection method (Jiang et al., 2019a,b). Requirements for inclusion and criteria for rejection were determined using an iterative process across patients, structures, and states. Data were first bandpassed at 60–120 Hz (sixth-order Butterworth filter with zero-phase shift), and the top 20% of 20 ms moving root-mean-squared peaks were detected. It was further required that the maximum  $z$  score of the analytic amplitude of the 70–100 Hz bandpass was  $>3$  and that there were at least three distinct oscillation cycles in the 120 Hz lowpassed signal, determined by shifting a 40 ms window in increments of 5 ms across  $\pm 50$  ms relative to the ripple midpoint and requiring that at least one window have at least three peaks. Adjacent ripples within 25 ms were merged. Ripple centers were determined as the time of the maximum positive peak in the 70–100 Hz bandpass. Ripple onsets and offsets were identified on each side of the center peak when the 70–100 Hz analytic amplitude fell below 0.75  $z$  scores. To reject epileptiform activities or artifacts, ripples were excluded if the absolute value of the  $z$  score of the 100 Hz highpass exceeded 7 or if they occurred within 2 s of a  $\geq 3$  mV/ms change in the broadband LFP. Ripples were also excluded if they fell within  $\pm 500$  ms of putative IISs, detected as described below. To exclude events that could be coupled across channels because of epileptiform activity, we excluded events that coincided with a putative IIS on any cortical or hippocampal SEEG channel included in the analyses. Events in SEEG recordings that had only one prominent cycle or deflection in the broadband LFP that manifested as multiple cycles above detection threshold in the 70–100 Hz bandpass were excluded if the largest valley-to-peak or

peak-to-valley absolute amplitude in the broadband LFP was 2.5 times greater than the third largest. For each channel, the mean ripple-locked LFP and mean ripple band were visually examined to confirm that there were multiple prominent cycles at ripple frequency (70–100 Hz) and the mean time-frequency plot was examined to confirm there was a distinct increase in power within the 70–100 Hz band. In addition, multiple individual ripples in the broadband LFP and 70–100 Hz bandpass from each channel were visually examined to confirm that there were multiple cycles at ripple frequency without contamination by artifacts or epileptiform activity. Channels that did not contain ripples that met these criteria were excluded from the study. Of note, a recent study has identified ripples based on these criteria in a patient without epilepsy (Rubin et al., 2022). The oscillation frequency of each ripple was computed by first counting the number of 70–100 Hz bandpass zero crossings (each representing half a cycle) during the ripple event and adding any remaining partial half cycle (i.e., the remaining phase angle over  $\pi$ ). The number of half cycles in the ripple was divided by 2 to calculate the total number of cycles during the ripple. Finally, the oscillation frequency in Hertz was calculated as the number of cycles divided by the ripple duration in seconds.

**Subtraction of unit spikes from LFPs.** One challenge in detecting high-frequency oscillations, such as ripples in the LFP recorded by a microelectrode, is that unit spikes may “bleed through” into the micro-LFP (Ray, 2015), thus resulting in the detection of spurious relationships between ripples and unit spikes. Although unit spikes are fast events, simply downsampling (which requires first low-passing to prevent aliasing) may not completely remove the influence of the action potential on the micro-LFP. To address this, we used a modified unit spike waveform subtraction technique (Pesaran et al., 2002). Specifically, the average spike waveform ( $-500$  to  $1600$   $\mu$ s around the trough) of each unit was subtracted from the unfiltered 30 kHz Utah Array micro-LFP of the same channel centered on each spike. The data were then downsampled to 1 kHz and ripple detection was performed as described above. We confirmed that this method led to the detection of true oscillations through extensive visual confirmation of events in the 30 kHz micro-LFPs.

**IIS detection and rejection.** Ripples and other sleep waves were excluded if they were within  $\pm 500$  ms from putative IIS detected as follows: A high-frequency score was computed by smoothing the 70–190 Hz analytic amplitude with a 20 ms boxcar function, and a spike template score was generated by computing the cross-covariance with a template IIS. The high-frequency score was weighted by 13, the spike score was weighted by 25, and an IIS was detected when these weighted sums exceeded 130. In each patient, detected IIS and intervening epochs

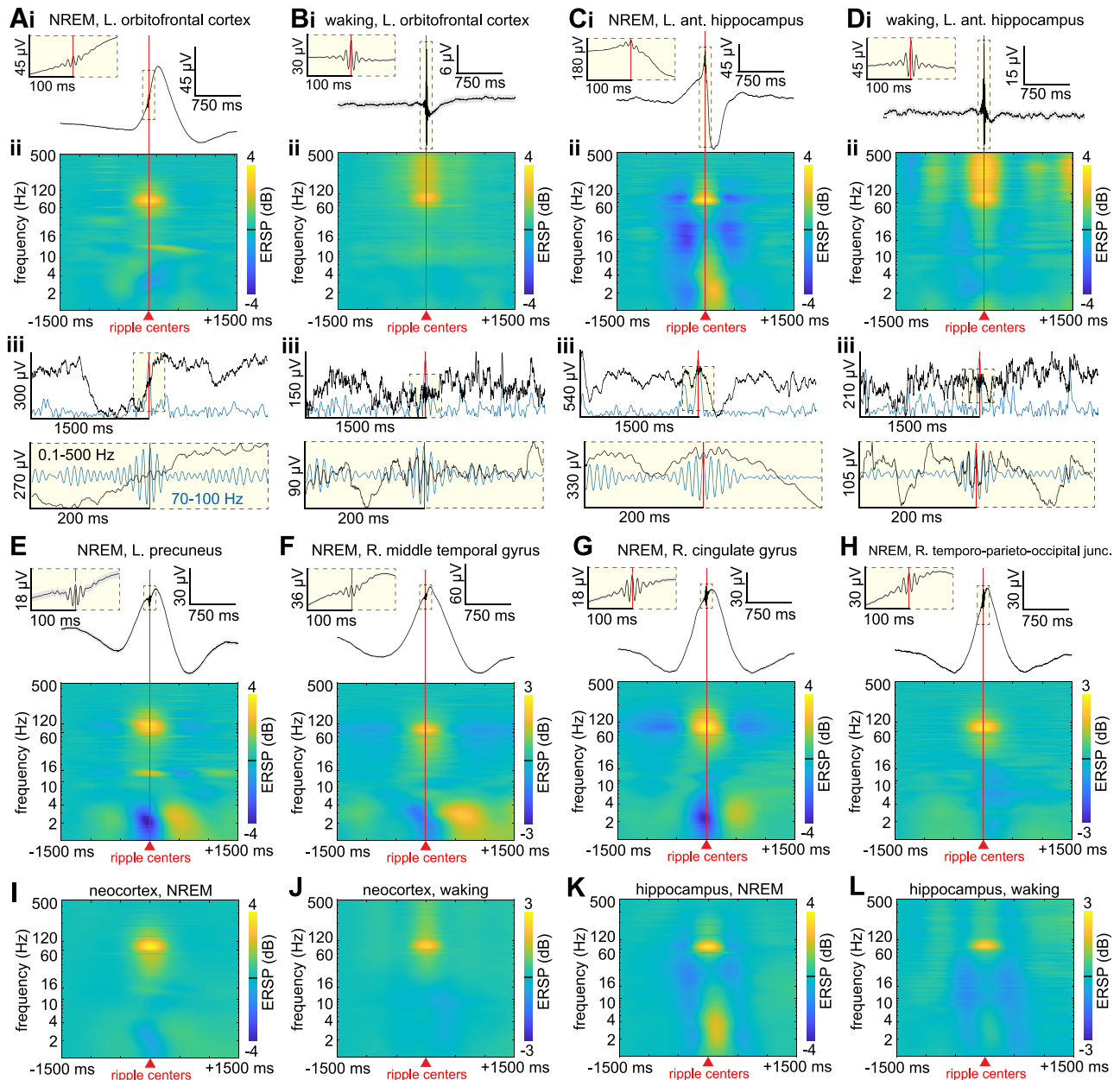


**Figure 2.** Cortical and hippocampal ripples are generated during NREM and waking. **A**, Orbitofrontal ripples from one channel during NREM. **Ai**, Average broadband LFP. **Aii**, Average time-frequency plot. **Aiii**, Example broadband unfiltered 3 s sweep (black) with 70–100 Hz bandpass analytic amplitude (blue) and below the same example, 400 ms sweep (black) with 70–100 Hz bandpass (blue). **B**, Same as in **A**, but during waking. **C**, Same as in **A**, but with hippocampal ripples (note ripple on sharp-wave peak). **D**, Same as in **C**, but during waking. **E–H**, Same as in **A**, but from other cortical regions. **I–L**, Grand average time-frequency plots across all channels in neocortex ( $N = 273$ ) during NREM (**I**) and waking (**J**), as well as in hippocampus ( $N = 28$ ) during NREM (**K**) and waking (**L**). Note the highly consistent and focal concentration of power centered at  $\sim 90$  Hz, the occurrence of cortical ripples on the down-to-upstate transition during NREM, and that some channels show increased power in the 10–16 Hz spindle band coinciding with the ripples. All plots represent ripples detected on bipolar SEEG channels. ERSP, Event-related spectral power.

were visually examined from hippocampal and cortical channels (when present) to confirm high detection sensitivity and specificity.

**Detection of downstates, upstates, and sleep spindles.** Downstates and upstates were detected as previously described (Jiang et al., 2019a,b), where the broadband LFP from each channel was bandpassed from 0.1–4 Hz (sixth-order Butterworth filter with zero-phase shift), and consecutive zero crossings separated by 0.25–3 s were selected. The top 10% amplitude peaks were selected, and the polarity of each signal was inverted if needed so that downstates were negative and upstates were positive, by ensuring that the average analytic amplitude of the 70–190 Hz bandpass within  $\pm 100$  ms around the peaks was greater for upstates than downstates. A total of 2,649,563 downstates were detected, with an average and SD (across channels) density (occurrence rate) of  $12.9 \pm 4.7 \text{ min}^{-1}$

and amplitude of  $-237.3 \pm 169.8 \mu\text{V}$ . A total of 2,922,211 upstates were detected with a density of  $14.6 \pm 4.7 \text{ min}^{-1}$  and amplitude of  $163.8 \pm 84.9 \mu\text{V}$ .

Spindles were detected as previously described (Hagler et al., 2018), where data were bandpassed at 10–16 Hz, then the absolute values were smoothed via convolution with a tapered 300 ms Tukey window, and median values were subtracted from each channel. Data were normalized by the median absolute deviation, and spindles were detected when peaks exceeded 1 for at least 400 ms. Onsets and offsets were marked when these amplitudes fell below 1. Putative spindles that coincided with large increases in lower (4–8 Hz) or higher (18–25 Hz) band power were rejected to exclude broadband events as well as theta bursts, which may extend into the lower end of the spindle range (Gonzalez et al., 2018). A

**Table 3. Cortical and hippocampal ripple characteristics by region in NREM and waking<sup>a</sup>**

Region	No. of patients	No. of channels	No. of ripples		Density (min <sup>-1</sup> )		Amplitude (μV)		Frequency (Hz)		Duration (ms)	
			NREM	Waking	NREM	Waking	NREM	Waking	NREM	Waking	NREM	Waking
Orbitofrontal	6	14	129680	211957	9.01 ± 2.74	4.83 ± 3.26	1.38 ± 0.27	2.35 ± 1.23	88.8 ± 0.7	89.2 ± 0.9	74.4 ± 5.6	65.1 ± 3.1
Prefrontal	8	37	287124	609692	9.28 ± 2.66	6.62 ± 3.11	1.68 ± 0.60	2.19 ± 0.86	89.0 ± 0.7	89.5 ± 0.7	72.7 ± 4.9	64.4 ± 3.9
Rolandic	13	25	174262	315588	8.84 ± 2.57	6.36 ± 3.39	1.91 ± 0.95	2.88 ± 2.13	89.1 ± 0.8	89.5 ± 0.5	76.8 ± 13.5	66.0 ± 5.6
Parietal	16	79	491431	855766	8.18 ± 2.68	5.13 ± 3.45	1.84 ± 0.66	2.56 ± 1.15	89.3 ± 0.9	89.6 ± 0.6	76.6 ± 7.4	66.6 ± 5.9
Occipital	8	14	94144	103609	8.71 ± 2.91	4.55 ± 3.10	2.05 ± 0.77	3.12 ± 1.25	89.0 ± 0.6	89.7 ± 0.5	80.2 ± 9.9	65.4 ± 4.3
Superior temporal/insula	10	20	182981	324005	8.99 ± 2.08	7.90 ± 4.16	1.57 ± 0.64	2.49 ± 1.32	88.9 ± 0.8	89.7 ± 0.6	76.3 ± 15.8	65.2 ± 4.8
Lateral temporal	15	47	295324	534754	6.89 ± 2.61	4.95 ± 3.35	1.28 ± 0.74	1.98 ± 1.38	89.1 ± 0.9	89.5 ± 0.7	76.6 ± 12.7	66.3 ± 6.1
Ventral temporal	14	34	224478	417057	8.58 ± 2.64	6.54 ± 2.82	1.94 ± 0.82	2.73 ± 1.73	88.8 ± 0.7	89.2 ± 0.9	78.0 ± 6.9	69.7 ± 8.3
Cingulate	3	3	27078	42804	9.31 ± 1.84	7.00 ± 2.17	1.25 ± 0.85	1.55 ± 0.97	90.0 ± 0.0	89.8 ± 0.7	90.7 ± 27.7	87.7 ± 40.1
Mean (total) of cortical channels	17	273	1906502	3415232	8.36 ± 2.69	5.77 ± 3.42	1.70 ± 0.75	2.46 ± 1.39	89.1 ± 0.8	89.5 ± 0.7	76.5 ± 10.1	66.6 ± 7.2
Hippocampus	17	28	147138	409734	6.95 ± 4.80	7.40 ± 5.47	5.76 ± 2.58	6.00 ± 3.16	85.7 ± 2.0	88.2 ± 1.4	87.5 ± 9.0	69.7 ± 7.9

<sup>a</sup>Cortical parcellation scheme is specified in Table 2. Values are counts or mean ± SD across channels (*N* = 273 cortical, *N* = 28 hippocampal) from SEEG Patients S1–S17.

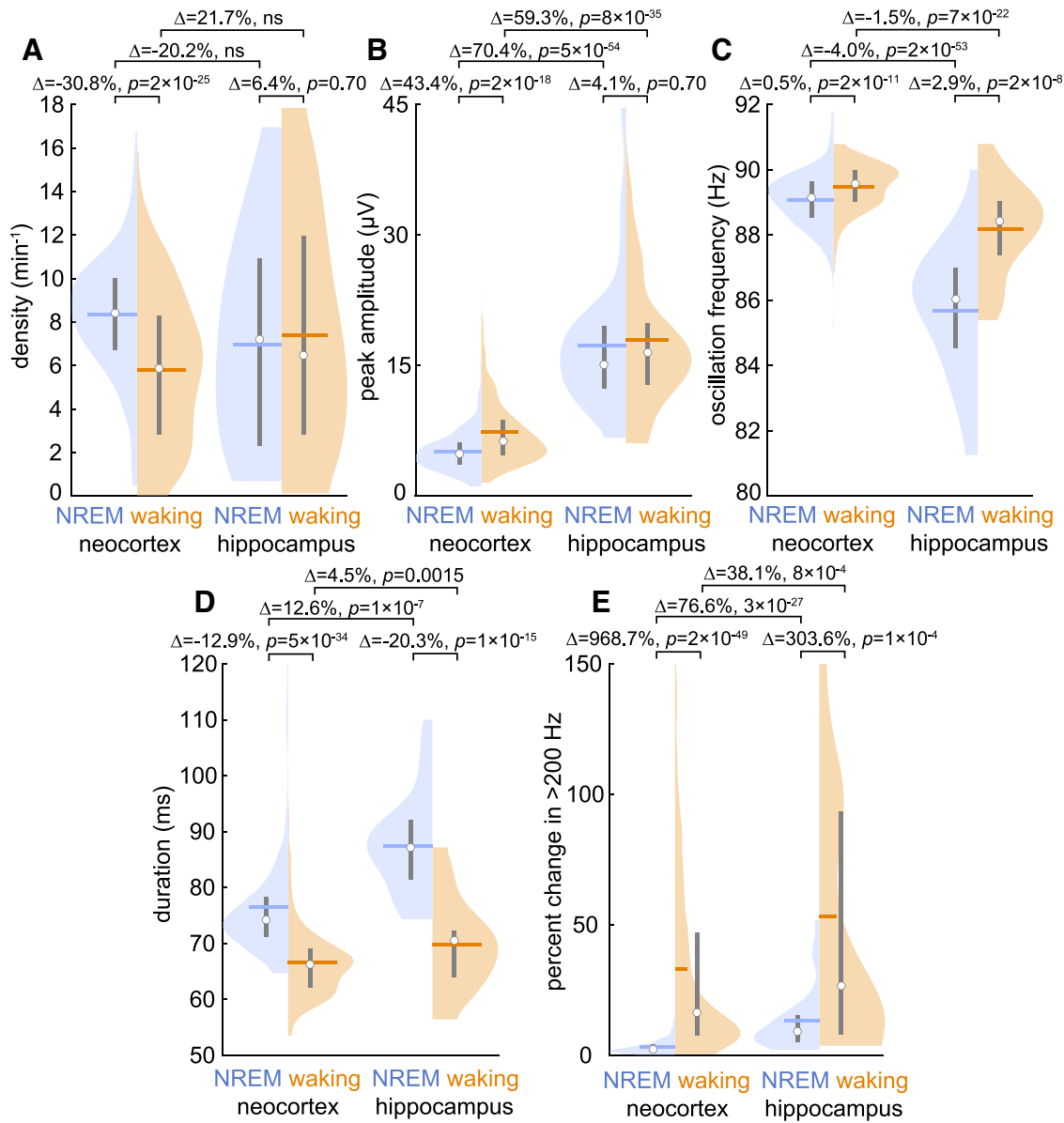


**Figure 3.** Neocortical and hippocampal ripple characteristics in NREM and waking. **A–E**, NREM and waking cortical ripple density (**A**), peak 70–100 Hz analytic amplitude (**B**), oscillation frequency (**C**), duration (**D**), and percent change in mean >200 Hz analytic amplitude during ripples compared with a –2 to –1 s baseline (**E**). Distributions are comprised of channel means (SEEG Patients S1–S17; *N* = 273 neocortical channels, *N* = 28 hippocampal channels). Circles represent medians. Horizontal lines indicate means. Vertical lines indicate interquartile ranges. FDR-corrected *p* values, linear mixed-effects models with *post hoc* analyses, patient as random effect. ns, Nonsignificant factor precluding *post hoc* analysis. For distributions across individual ripples, see Figure 4. For distributions across individual patients, see Figure 5. Figure 1B, C shows that the ~90 Hz ripple frequency we measured is not because of filtering including the detection bandpass.

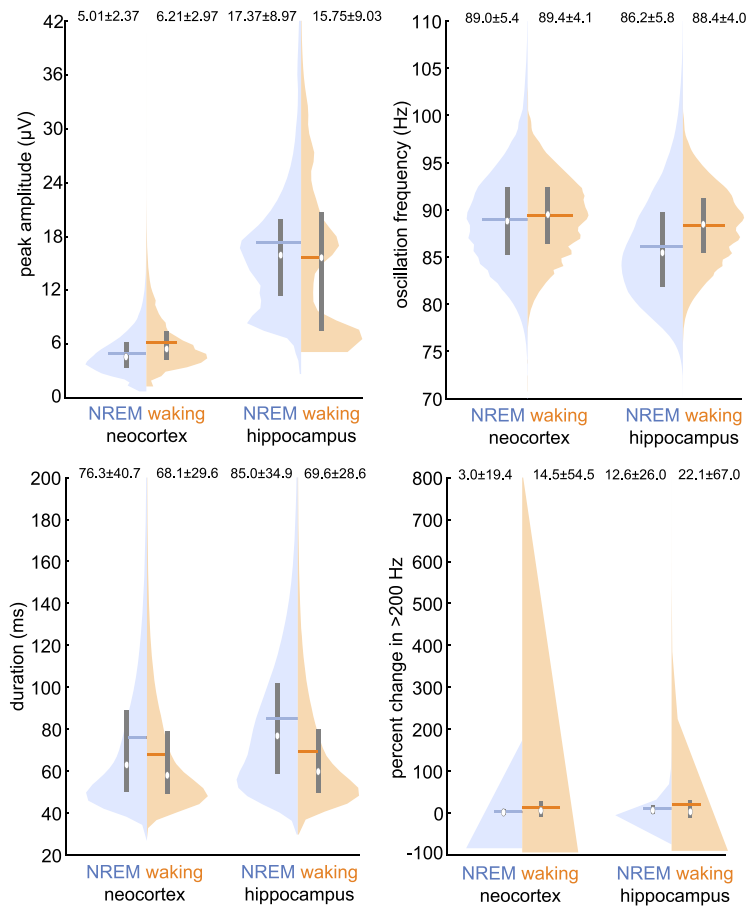


**Figure 4.** Characteristics of individual cortical ripples. Histograms of ripple characteristics across individual events ( $N_{NREM} = 1,906,502$ ,  $N_{waking} = 3,415,232$ ) from all channels ( $N = 273$  cortical,  $N = 28$  hippocampal) from all SEEG patients (S1–S17). Values are mean ± SD. Circles represent medians. Horizontal lines indicate means. Vertical lines indicate interquartile ranges.

total of 694,168 spindles were detected with an average and SD (across channels) density of  $3.0 \pm 3.0 \text{ min}^{-1}$ , amplitude of  $29.1 \pm 13.5 \mu\text{V}$ , oscillation frequency of  $12.4 \pm 0.7 \text{ Hz}$ , and duration of  $633.5 \pm 67.2 \text{ ms}$ .

**Ripple temporal relationships.** Peri-cortical ripple time histograms of cortical sleep waves on the same channel were computed. Event counts were found in 50 ms bins for sleep waves within  $\pm 1500 \text{ ms}$  around cortical ripple centers at  $t = 0$ . A null distribution was generated by shuffling the event times relative to the ripples at  $t = 0$  within this 3 s window 200 times each. Pre-FDR  $p$  values were computed by comparing the observed and null distributions within each bin over  $\pm 1000 \text{ ms}$  for cortical sleep waves. These  $p$  values were then FDR-corrected for the number of channels across patients multiplied by the number of bins per channel (Benjamini and Hochberg, 1995). A channel was considered to have a significant modulation if there were three or more consecutive bins with FDR-corrected  $p$  values less than  $\alpha = 0.05$ . Whether events were leading or lagging cortical ripples at  $t = 0$  was computed for each channel with a two-sided binomial test with expected value of 0.5, using event counts in the 1000 ms before versus 1000 ms after  $t = 0$  for sleep waves. Plots had 50 ms Gaussian smoothed event counts with 50 ms bins.

Conditional probabilities of a ripple given the following sleep waves or their sequences were computed: downstate, spindle, upstate, downstate-spindle, and spindle-upstate. A ripple given a spindle ( $R | SS$ ) was determined if the ripple center occurred during the spindle (average spindle duration was 634 ms). A ripple was considered to precede an upstate ( $R | US$ ) or follow a downstate ( $R | DS$ ) if the ripple center occurred within 634 ms before or after the peak of the upstate or downstate, respectively.

**Unit detection, classification, quality, and isolation.** Unit detection and classification were performed according to our published procedures

(Peyrache et al., 2012; Chan et al., 2014; Dehghani et al., 2016; Le Van Quyen et al., 2016; Teleńczuk et al., 2017; Eichenlaub et al., 2020; Dickey et al., 2021). Data were bandpassed at 300–3000 Hz and putative unit spikes were detected when the filtered signal exceeded 5 times the estimated SD of the background noise. Units were  $k$ -means clustered using the first three principal components of each spike. Overlaid spikes were examined visually and those with abnormal waveforms were excluded. Based on their waveforms, firing rates, and autocorrelograms, action potentials were clustered as arising from putative PYs or INs. PYs had spike rates of  $\sim 0.1$ – $0.8 \text{ Hz}$ , long valley-to-peak and half-width intervals, sharp autocorrelations, and bimodal interspike interval (ISI) distributions, reflecting a propensity to fire in bursts. By contrast, INs had spike rates of  $\sim 1$ – $5 \text{ Hz}$ , short valley-to-peak and half-width intervals, broad autocorrelations, and a predominantly unimodal ISI distribution. The Utah Array patient included in the study had 69 PY with a total of 231,922 spikes, as well as 23 IN with a total of 462,246 spikes. The average and SD PY valley-to-peak amplitude was  $44.8 \pm 12.9 \mu\text{V}$ , spike rate was  $0.28 \pm 0.17 \text{ Hz}$ , valley-to-peak width was  $0.49 \pm 0.5 \text{ ms}$ , half-peak width was  $0.62 \pm 0.04 \text{ ms}$ , and bursting index was  $0.03 \pm 0.02$ . The average and SD IN valley-to-peak amplitude was  $28.9 \pm 11.9 \mu\text{V}$ , spike rate was  $1.67 \pm 1.63 \text{ Hz}$ , valley-to-peak width was  $0.29 \pm 0.05 \text{ ms}$ , half-peak width was  $0.34 \pm 0.05 \text{ ms}$ , and bursting index was  $0.01 \pm 0.01$ . Valley-to-peak amplitude, spike rate, valley-to-peak width, half-peak width, and bursting index were all significantly different between PY and IN ( $p < 0.0001$ , two-sided two-sample  $t$  test).

Single-unit quality and isolation were confirmed according to previously established guidelines (Kamiński et al., 2020). Unit spikes were verified to well exceed the noise floor based on large peak signal-to-noise ratios (PY:  $10.1 \pm 3.4$ ; IN:  $5.9 \pm 3.1$ ). Since the neuronal spiking refractory period is  $\sim 3 \text{ ms}$ , the percent of ISIs  $< 3 \text{ ms}$  estimates the degree of single-unit contamination by spikes from different units, which was very low among the units included in this study (PY:  $0.12 \pm 0.15\%$ ; IN:  $0.31 \pm 0.50\%$ ). Furthermore, single units detected on the same contact were highly separable according to their projection distances (Pouzat et al., 2002) (PY:  $49.2 \pm 25.8 \text{ SD}$ ; IN:  $50.9 \pm 28.6 \text{ SD}$ ). Last, temporal stability of unit spikes over time was confirmed based on consistency of the mean waveform shape and amplitude of each unit across recording quartiles.

**Analyses of unit spiking during ripples.** Unit spiking was analyzed with respect to local ripples detected on the same contact. Ripple phases of unit spikes were determined by finding the angle of the Hilbert transform of the 70–100 Hz bandpassed signal (zero-phase shift) at the times of the spikes. The circular mean ripple phase was determined for each unit according to Berens (2009). Phase analyses were only performed on units that had at least 30 spikes during local ripples. The Rayleigh test was used to assess for unimodal deviation from uniformity of the circular mean phases across units. PY–PY and PY–IN unit pair cofiring within 5 ms was assessed based on Dickey et al. (2021). To evaluate cofiring when there was a ripple at either or both sites versus baseline when there were no ripples occurring, we randomly selected non-ripple epochs matched in number and duration to the ripples but during which there were no ripples detected on either channel. Cofiring during ripples with observed versus random spike times was computed by shuffling the spike times of each unit within the intervals of the ripples.

**Experimental design and statistical analyses.** All statistical tests were evaluated with  $\alpha = 0.05$ . All  $p$  values involving multiple comparisons were FDR-corrected according to Benjamini and Hochberg (1995). FDR

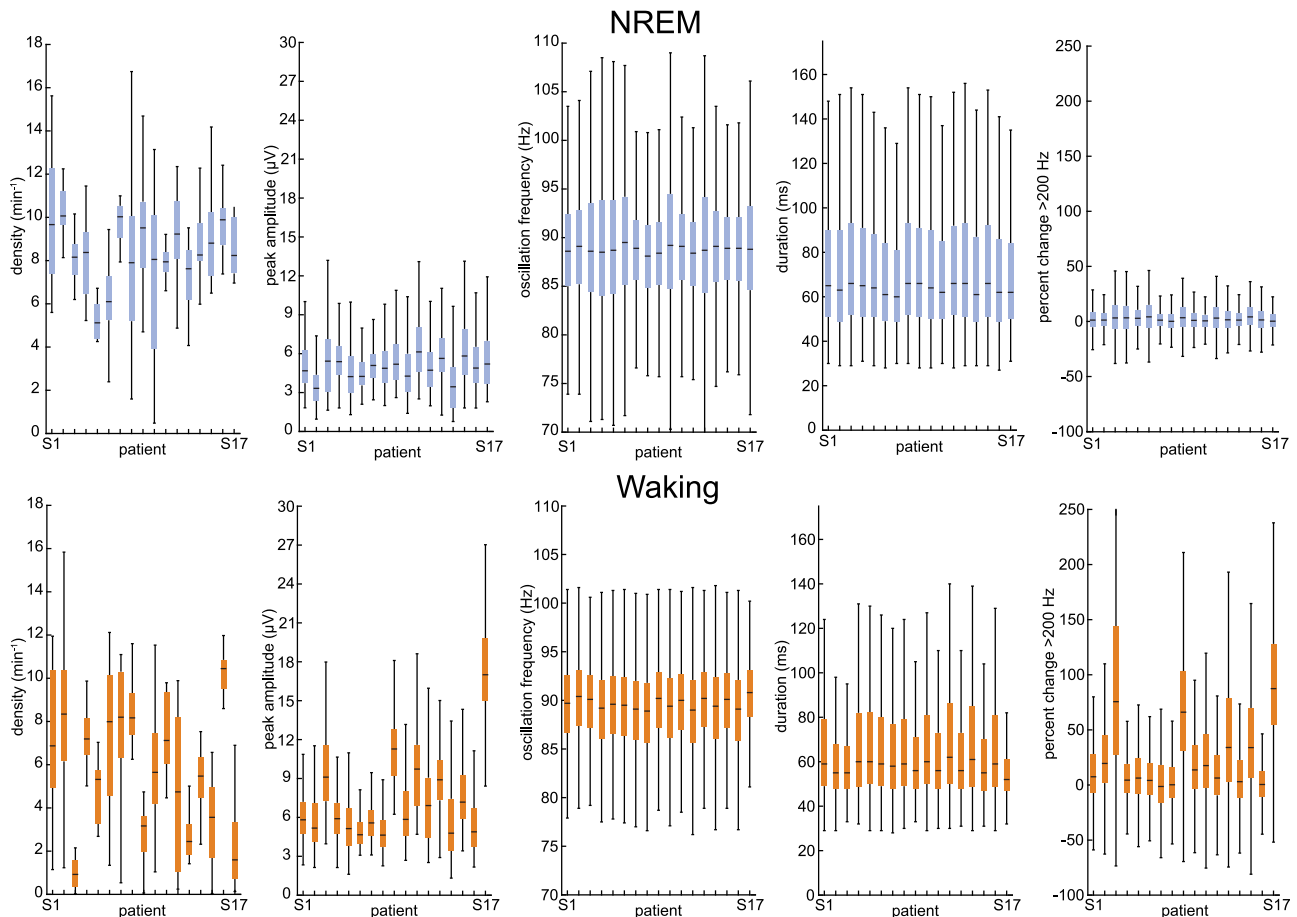


**Figure 5.** Cortical ripple characteristics by patient. Cortical ripple characteristics are consistent across patients (S1–S17). Horizontal lines indicate medians. Boxes represent interquartile ranges. Whiskers represent  $1.5 \times$  interquartile range.

corrections across channel pairs were done across all channels pairs from all patients included in the analysis. Box-and-whisker plots show median, mean, and interquartile range, with whiskers indicating  $1.5 \times$  interquartile range with outliers omitted. Kernel density plots were produced using methods from Bechtold (2016). Significance and shuffling statistics of peri-ripple time histograms were computed as described above. Unit spiking statistics were computed as described above.

Statistical comparisons between ripple characteristics were performed using two-sided paired or two-sided two-sample *t* tests between channel means. Differences in ripple characteristics between states (NREM or waking) or regions (cortex or hippocampus) were determined using linear mixed-effects models with state and region as fixed effects and patient as a random effect, according to the following model:

$$\text{characteristic} \sim \text{region} + \text{state} + (1 | \text{patient}) \quad (1)$$

Factors that had  $p < 0.05$  then underwent *post hoc* testing with the following models. These *p* values were then FDR-corrected for multiple comparisons.

$$\text{characteristic} \sim \text{region} + (1 | \text{patient}) \quad (2)$$

$$\text{characteristic} \sim \text{state} + (1 | \text{patient}) \quad (3)$$

Significance of linear correlations (i.e., ripple characteristics vs myelination index or hippocampal connectivity density) was assessed when there were at least 10 data points using linear mixed-effects models with patient as random effect, according to the following model:

$$\text{characteristic} \sim \text{connectivity} + (1 | \text{patient}) \quad (4)$$

**Data availability.** The deidentified raw data that support the findings of this study are available from the corresponding authors on reasonable request provided that the data sharing agreement and patient consent permit that sharing.

**Code availability.** The code that supports the findings of this study is available from the corresponding authors on reasonable request.

## Results

### Ripples are ubiquitous across states and structures with a characteristic and focal frequency ( $\sim 90$ Hz) and duration ( $\sim 70$ ms)

Ripples were detected in intracranial cortical and hippocampal SEEG recordings from 17 patients undergoing monitoring for seizure focus localization (Table 1). Bipolar transcortical derivations ensured measurement of locally generated LFPs. Ripples were detected exclusively from nonlesional, nonepileptogenic regions and were required to have at least three cycles of increased 70–100 Hz amplitude without contamination by epileptiform activity or artifacts (Fig. 1A). Recording epochs and channels with possible contamination by epileptiform activity were rigorously rejected. Ripples were found during both waking and NREM in all cortical areas sampled (Fig. 2A,B,E–J; Table 3) as well as the hippocampus (Fig. 2C,D,K,L; Table 3).

Across states and cortical regions, ripple frequency was remarkably consistent at  $\sim 90$  Hz. Specifically, mean cortical ripple frequency within region ranged from 88.8–90.0 Hz during

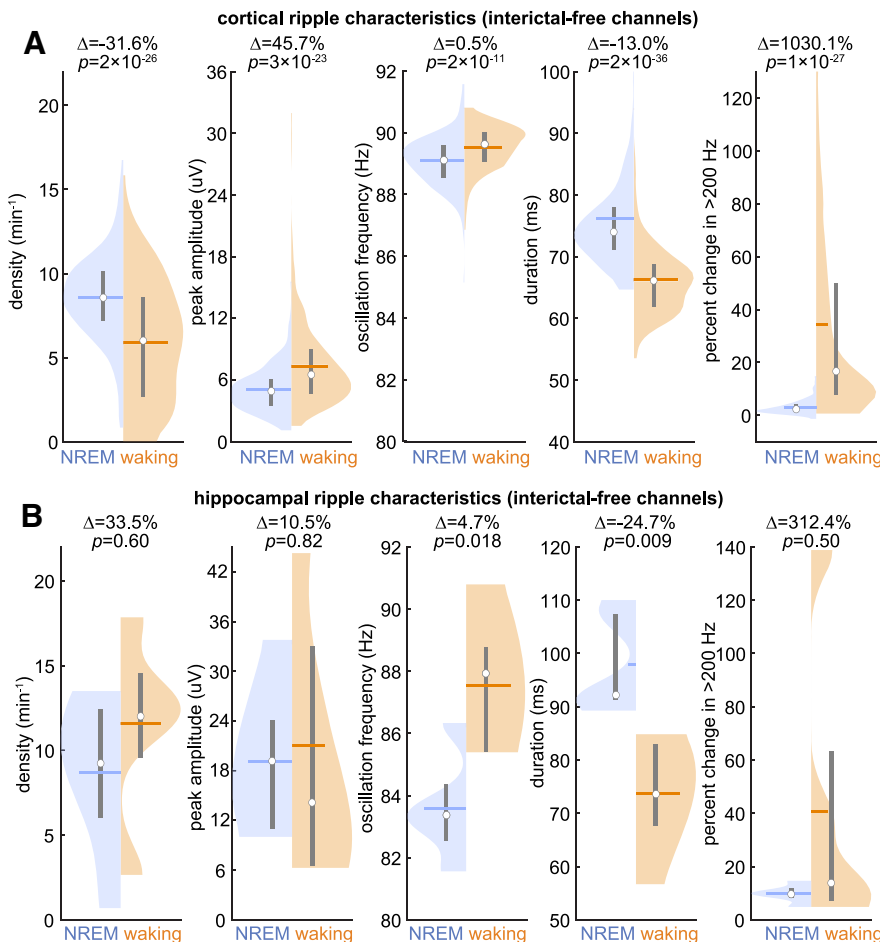


**Figure 6.** Characteristics of ripples detected on interictal-free channels. **A**, NREM and waking cortical ripple density, peak 70–100 Hz analytic amplitude, oscillation frequency, duration, and percent change in mean  $>200$  Hz analytic amplitude in interictal-free cortical channels ( $N = 232$  channels; Patients S1–S17). **B**, Same as in **A**, but with interictal-free hippocampal channels ( $N = 5$  channels; Patients S4, S6, S9, and S17).

NREM and 89.2–89.8 Hz during waking (Table 3; Fig. 3). The mean  $\pm$  SD ripple oscillation frequency across all cortical channel means during NREM was  $89.1 \pm 0.8$  Hz and during waking was  $89.5 \pm 0.7$  Hz. These data are also presented as histograms of individual ripple characteristics (amplitude, frequency, duration, associated changes in  $>200$  Hz amplitude) in Figure 4 as well as individual patients in Figure 5. The basic characteristics of cortical ripples were very similar in a supplemental analysis which only included cortical channels free of IISs (Fig. 6A).

Oscillation frequency was not only highly consistent at  $\sim 90$  Hz across ripples, but increased amplitude was highly concentrated during ripples at  $\sim 90$  Hz in broadband recordings, with a steep drop-off in amplitude at higher and lower frequencies. This focal power increase, which is especially prominent during NREM, can be seen in example channels (Fig. 2A,E–H) as well as grand average time-frequency plots that are averages across all channel averages of all ripples (Fig. 2I–L).

We conducted supplementary analyses to examine whether this regularity and focality of ripple frequency could be because of our method of detecting them. First, we conducted a complete reanalysis of all SEEG channels and epochs using two different frequency ranges for ripple detection and selection. One used a detection bandpass from 70 to 100 Hz as in our primary analysis, and the other expanded the detection bandpass to 65–120 Hz. Mean  $\pm$  SD NREM ripple oscillation frequency across channels

( $N = 273$ ) from all SEEG patients (S1–S17) is highly similar when using either a 70–100 Hz bandpass (mean  $\pm$  SD =  $89.1 \pm 0.8$  Hz) or a 65–120 Hz bandpass ( $92.7 \pm 2.2$  Hz) (Fig. 1B). Furthermore, we verified that the 60 and 120 Hz notch filters (to remove line noise) as well as the 70–100 Hz bandpass did not artificially produce a peak in power at  $\sim 90$  Hz (Fig. 1C). Thus, the ripple oscillation frequency of  $\sim 90$  Hz appears to be physiologic rather than being driven by specific detection methods.

The mean ripple duration was also remarkably consistent ( $\sim 70$  ms) across states and cortical regions (Table 3). The duration and consistency are not explained by the detection requirement of having at least 3 cycles (which at 90 Hz is 33.3 ms), suggesting that this duration is also a physiological characteristic. Other characteristics, including density (NREM:  $8.36 \pm 2.69 \text{ min}^{-1}$ , waking:  $5.77 \pm 3.42 \text{ min}^{-1}$ ), peak amplitude (NREM:  $5.10 \pm 2.25 \mu\text{V}$ , waking:  $7.38 \pm 4.17 \mu\text{V}$ ), and change in  $>200$  Hz amplitude (NREM:  $3.09 \pm 2.75\%$ , waking:  $33.02 \pm 36.90\%$ ) were also highly similar across channels (Figs. 2, 3). Ripple characteristics were also consistent across patients (Fig. 5). However, small but significant differences were noted between regions, cortex versus hippocampus, and NREM versus waking, which are described below.

### Ripples exhibit small but significant differences between cortex and hippocampus

Human hippocampal ripples have previously been selected using a variety of methods (for review, see Jiang et al., 2019c). In our previous studies, we required that ripples be superimposed on sharp waves (characteristic of anterior hippocampus) (Jiang et al., 2019a) or spindles (characteristic of posterior hippocampus) (Jiang et al., 2019b). In the current study, we reanalyzed these data using exactly the same criteria and procedures as we used for detection and selection of cortical ripples, so as to avoid any methodological ambiguities; that is, we did not require the presence or absence of any associated lower-frequency LFP signature. Using the same detection criteria, we found that cortical and hippocampal ripples share the same basic characteristics with relatively small differences. The basic hippocampal ripple characteristics were very similar in a supplemental analysis, which only included hippocampal channels free of IISs (Fig. 6B). During NREM, hippocampal ripples had average time-frequency plots (Fig. 2C,K) that resembled the corresponding cortical plots (Fig. 2A,E–I) in having concentrated oscillatory activity at  $\sim 90$  Hz, but differed in being superimposed on the peak of a local sharp-wave-ripple rather than occurring just before the local upstate as is seen in the cortex. During waking, average time-frequency plots of hippocampal (Fig. 2D,L) and cortical (Fig. 2B,J) ripples again show concentrated oscillatory activity at  $\sim 90$  Hz, but also with activity that stretches into higher

frequencies as noted above. Statistical analyses (Fig. 3) revealed several differences which, although small, were nonetheless significant, attributable to the large numbers of channels. Specifically, compared with cortical ripples, hippocampal ripples were on average: slightly less dense during NREM, and more dense during waking; slightly lower frequency, especially during NREM (but still  $<3$  Hz difference); longer duration, especially during NREM (but  $<10$  ms difference); larger amplitude (by  $\sim 2.5\times$ ); and accompanied by a smaller but still significant increase in  $>200$  Hz amplitude during waking compared with NREM. In addition, cortical ripple characteristics were not significantly correlated with the hippocampal connectivity density to their local parcel (Fig. 7). Overall, cortical and hippocampal ripples appear to be very similar, except notably in their amplitudes and associated slower waves during NREM (Fig. 2; Fig. 8A–F).

### Ripples can be distinguished from high-frequency limbic oscillations

Oscillatory activity  $>60$  Hz in humans has been studied previously, mainly in the hippocampus in relation to epilepsy. Le Van Quyen et al. (2010) reported likely nonpathologic activity, mainly from parahippocampal gyrus sites. They imposed a minimum duration of 100 ms, which would have eliminated the vast majority of the events that we studied (Figs. 3D, 4), and is longer than those previously reported for human hippocampal ripples (Jiang et al., 2019c), human cortical ripples (Vaz et al., 2019), and rodent hippocampal ripples (Buzsáki, 2015). In addition, being on average  $\sim 7\times$  longer than the events we describe here, those described by Le Van Quyen et al. (2010) also differ in that they contain several oscillatory frequencies (whereas those described here are strongly centered at  $\sim 90$  Hz) and have larger amplitudes. Their events are similar, however, in being related to upstates, and in modulating unit firing (see below). We were therefore interested in determining the relationship between the mainly parahippocampal events described by Le Van Quyen et al. (2010) and the widespread cortical events described here. We subselected our parahippocampal channels ( $N=5$  channels from 5 patients), and implemented the selection criteria described by Le Van Quyen et al. (2010): data were bandpassed at 40–120 Hz, minimum event duration was 100 ms, and otherwise events were detected as described in Materials and Methods. Using these selection criteria, we found very low densities of events. The average ripple density of parahippocampal channels during NREM using our criteria was  $9.08 \text{ min}^{-1}$  (range:  $7.23\text{--}10.77 \text{ min}^{-1}$ ), whereas that using the Le Van Quyen et al. (2010) detection criteria was only  $0.40 \text{ min}^{-1}$  (range:  $0\text{--}1.53 \text{ min}^{-1}$ ). Thus, the

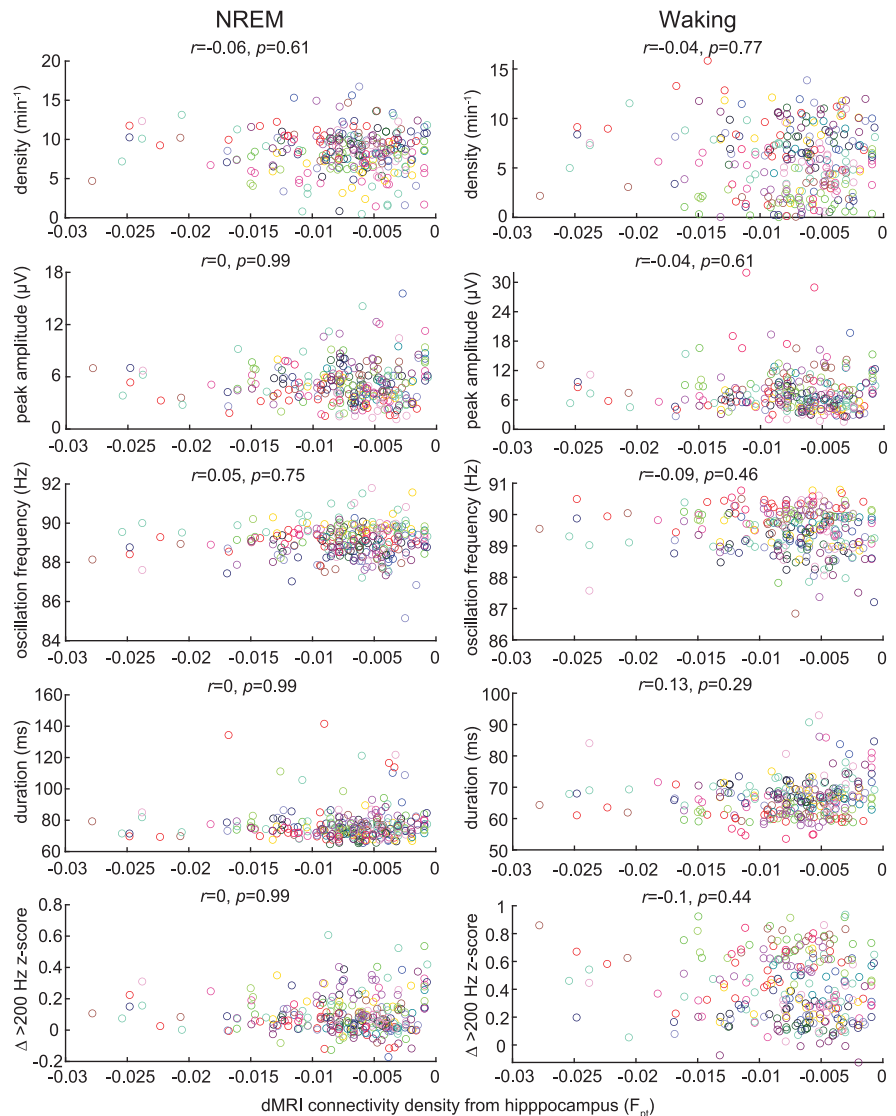


**Figure 7.** Cortical ripple characteristics versus estimated hippocampo-cortical connectivity density. Cortical ripple density, peak 70–100 Hz analytic amplitude, oscillation frequency, duration, and  $>200$  Hz amplitude modulation ( $N=273$  channels from Patients S1–S17) as a function of the connectivity density (Rosen and Halgren, 2021) between the hippocampus and each cortical parcel. The absence of significant correlations suggests that cortical ripples are related to corticocortical integration rather than being driven primarily by the hippocampus.

events described here do not correspond to those previously reported by Le Van Quyen et al. (2010).

### Ripples exhibit small but significant differences between primary sensory-motor and association cortices

Previous work in sleeping rats (Khodagholy et al., 2017) and waking humans (Vaz et al., 2019) found cortical ripples to be more common in association areas than in early sensory and motor regions where they were absent or infrequent. In contrast, we found that ripple density, amplitude, and accompanying  $>200$  Hz amplitude (a proxy for unit firing) (Mukamel et al., 2005) in primary cortex were all significantly higher than in association areas, as indicated by a positive correlation with the myelination index (Fig. 8G–I) (Rosen and Halgren, 2021). Oscillation frequency and duration were not correlated with myelination index (Fig. 9). In some cases, this effect was small, for example, explaining only 1.7% of the variance in density during waking

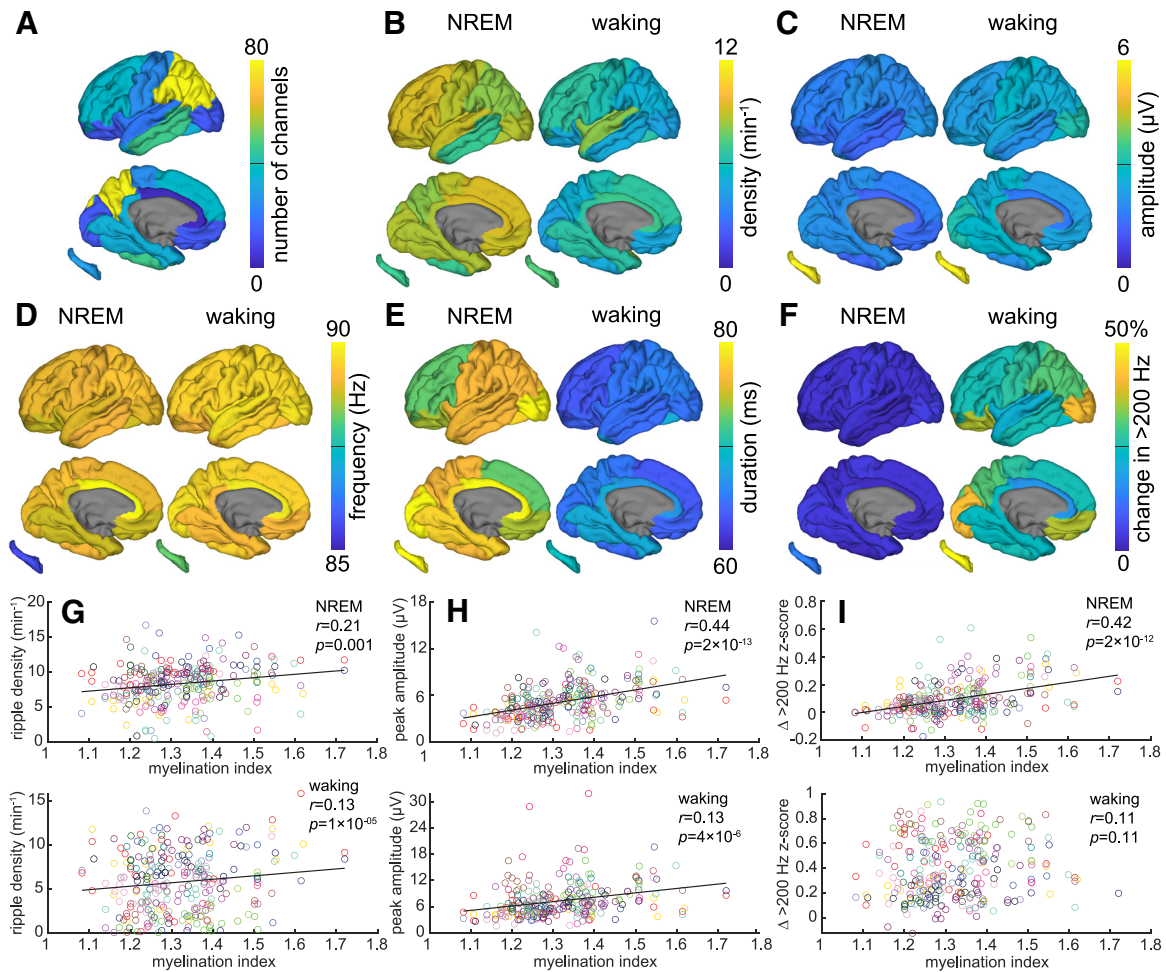


**Figure 8.** Distributions of ripple characteristics across the cortex and hippocampus in NREM and waking. **A–F**, Cortical maps with hippocampal map insets of channel coverage (**A**) as well as NREM and waking mean ripple densities (**B**), peak 70–100 Hz analytic amplitudes (**C**), oscillation frequencies (**D**), durations (**E**), and changes in mean >200 Hz analytic amplitude during ripples compared with baseline (–2 to –1 s) (**F**) (SEEG Patients S1–S17;  $N = 273$  channels). Left and right hemisphere channels were mapped onto a left hemisphere template. The parcellation scheme (specified in Table 2) is low resolution, and more extensive sampling may detect more spatially differentiated response characteristics. Values for each cortical region are reported in Table 3. **G, H**, Average cortical ripple density (**G**) and amplitude (**H**) by channel were significantly correlated with cortical parcel myelination index (i.e., lower densities and amplitudes in association compared with primary areas) (Rosen and Halgren, 2021) during NREM and waking (linear mixed-effects models with patient as random effect, FDR-corrected  $p$  values). Colors represent individual patients. **I**, Same as in **G, H**, but with change in mean >200 Hz amplitude z scores, for which there was a significant correlation during NREM but not waking.

and 4.4% during NREM. In other cases, the effect was substantial, for example, explaining 19.4% of the variance in amplitude during NREM. Comparing NREM and waking, in NREM there was a significantly stronger correlation between myelination index and density ( $p = 0.02$ ,  $t = 2.1$ ), amplitude ( $p = 8 \times 10^{-4}$ ,  $t = 3.2$ ), and >200 Hz modulation ( $p = 2 \times 10^{-6}$ ,  $t = 4.7$ ; one-sided paired  $r$  test; MATLAB: *r\_test\_paired*) (Steiger, 1980). In sum, human cortical ripples appear to be modestly more numerous and robust in sensory and motor than association areas.

### Ripples exhibit small but significant differences between NREM and waking

Most cortical and hippocampal ripple characteristics were similar between NREM and waking (Fig. 3; Table 3), but because of the large numbers of events, even small differences were significant. Considering only differences >10%, cortical ripple density was 31% higher and amplitude was 43% lower during NREM than waking. Ripple duration was 13% higher in the cortex and 20% higher in the hippocampus during NREM than waking. The most striking differences were the percent change in mean >200 Hz amplitude during ripples compared with a –2 to –1 s

baseline (Fig. 3E), which increased 969% from NREM to waking in the cortex, and 304% in the hippocampus. This difference is clearly seen to be broadband in the waking ripple triggered time-frequency plots from the cortex (Fig. 2Bii,I) and hippocampus (Fig. 2Dii,I), and thus would typically be interpreted not as an oscillation, but as an indication of increased multiunit activity. Thus, compared with waking, cortical ripples are somewhat denser, longer, and smaller in NREM; hippocampal ripples are also longer. The only major difference is that both cortical and hippocampal ripples appear to be associated with a much larger increase in putative multiunit activity during waking than NREM.

### Cortical ripples lock to sleep waves crucial for memory consolidation

Oscillation couplings are important for memory consolidation (Lathoumane et al., 2017). Previous studies have shown that cortical ripples occur on upstate and spindle peaks in cats (Grenier et al., 2001) and rats (Khodagholy et al., 2017), but these relationships have not been evaluated in humans. We detected downstates and upstates, with polarities determined based on

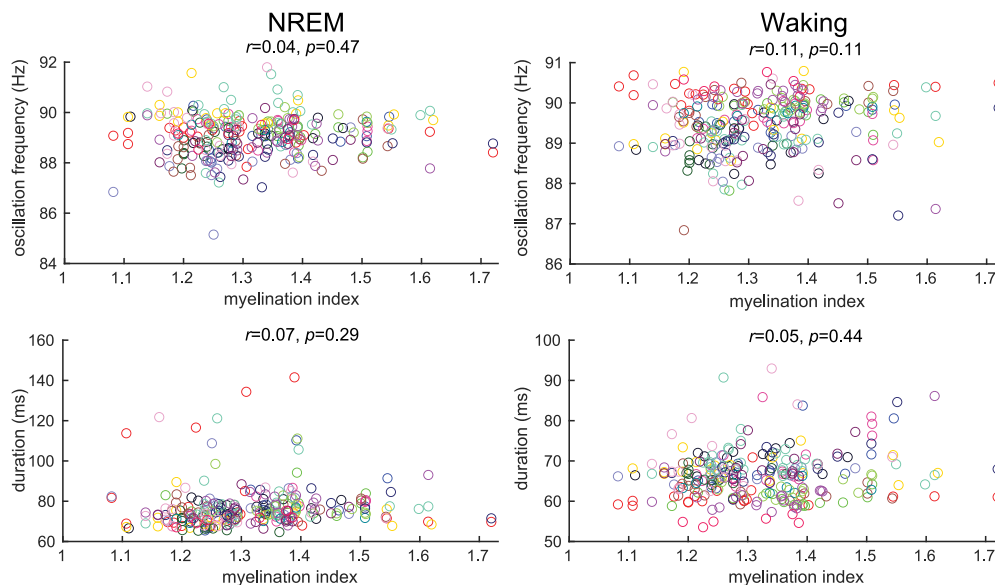


**Figure 9.** Cortical ripple oscillation frequency and duration versus myelination index. Neither cortical ripple oscillation frequency nor duration was significantly correlated with myelination index (Rosen and Halgren, 2021) during NREM or waking (linear mixed-effects models with patient as random effect, FDR-corrected  $p$  values,  $N = 273$  channels from Patients S1–S17). Colors represent individual patients. Notably, higher myelination indices correspond to primary, whereas lower myelination indices correspond to associative cortical regions.

associated high-frequency activity (for details, see Materials and Methods), as well as spindles, and found that cortical ripples were precisely coupled to the sequence of sleep waves described above (Fig. 10; Table 4). Specifically, in 95% of cortical channels, ripples were significantly associated with downstates and upstates (Fig. 10*B,D,E*), usually on the down-to-upstate transition, as seen in individual trials (Figs. 2*Aiii*, 10*A*), and in ripple-triggered averages of the broadband LFP (Fig. 2*Ai,E–H*). Peri-ripple histograms show that, on average, cortical ripple centers occurred 450 ms after downstate maxima and 100 ms before upstate maxima (Fig. 10*B,D–G*). Less frequently, ripples occurred during spindles (significant association in 29% of channels; Fig. 10*C,E*), as seen in individual trials (Fig. 10*A*), and in peri-ripple time-frequency plots (Fig. 2*Aii,E*). Peri-ripple histograms show that spindles began on average 225 ms before the cortical ripple center, indicating that ripples tend to occur during spindles (Fig. 10*C,E–G*). The probability of ripples occurring during spindles preceding upstates was greater than that for ripples occurring during spindles, or before upstates (Fig. 10*H*). These results suggest that the timing of cortical ripples during NREM is appropriate for facilitating consolidation, guided by a sequential activation of sleep waves.

#### PY firing precedes IN firing at cortical ripple peaks

Using microelectrode array recordings from granular/supragranular layers of lateral temporal cortex during NREM, we detected ripples (Fig. 11*A*) as well as action potentials, which were sorted into those arising from putative single PY or IN units. The mean  $\pm$  SD ripple oscillation frequency across microelectrode channels ( $N = 72$ ) was  $89.6 \pm 1.4$  Hz, and across individual ripples ( $N = 50,967$ ) was  $90.1 \pm 5.2$  Hz. We found that INs had a strong tendency to fire at the peak of the ripple, whereas PYs fired shortly before (Fig. 11*B*). We have previously shown that, in humans, upstates (Csicsvari et al., 2010) and spindles (Dickey et al., 2021) are associated with increased unit firing rates. Since cortical ripples are precisely coupled to these events (Fig. 10), their occurrence on upstates and spindles implies an underlying

phasic depolarization, which can generate  $\sim 90$  Hz oscillations in computational and experimental models via PY–IN feedback inhibition (Bazhenov et al., 2008; Buzsáki, 2015). Depolarization causes basket cells to fire synchronously, inhibiting other basket cells and pyramids via GABA<sub>A</sub>. Pyramids fire on recovery, exciting basket cells as they recover, leading to another cycle. As this model would predict, we found that PYs and INs were strongly phase-locked to cortical ripples (Fig. 11*B*), with PY significantly leading IN spiking (Fig. 11*C,D*). Furthermore, INs fired at the ripple peak, when pyramidal somatic inhibition would be maximal, as found in cats (Grenier et al., 2001). Similarly, ripple amplitude was higher in waking than NREM (Figs. 3*B*, 8*C*), consistent with relative depolarization of pyramidal membrane potential during waking. Phasic depolarization during waking ripples was also suggested by increased  $>200$  Hz amplitude (Figs. 2*B,J*, 3*E*, 8*F*). Thus, human cortical ripples are associated with strong tonic and phase-locked increases in PY and IN firing, and are likely generated by a sudden depolarization triggering PY–IN feedback oscillations (Fig. 11*E*).

#### Cortical ripples group cofiring with timing optimal for STDP

The increased tonic and phase-locked unit firing and occurrence of ripples on spindles on the down-to-upstate transition suggest that ripples may facilitate cortical plasticity (Dickey et al., 2021). This could occur through short latency cofiring between units that leads to STDP. Indeed, we found a large increase during ripples of short latency ( $<5$  ms) cofiring between PY–PY unit pairs and PY–IN unit pairs (Fig. 11*F*). Specifically, there was an increase in cofiring during ripples versus nonripples (PY–PY: 7.16-fold increase,  $p = 2 \times 10^{-159}$ ,  $N = 4638$ ,  $t = 28.0$ ; PY–IN: 9.78-fold increase,  $p = 8 \times 10^{-99}$ ,  $N = 1561$ ,  $t = 22.7$ ; one-sided paired  $t$  test). Nonripple comparison periods were randomly selected epochs between ripples matched in number and duration.

In order to test whether this increase in cofiring was not simply because of an increase in the overall firing rates of units during ripples, or even their rhythmicity, but rather a specific

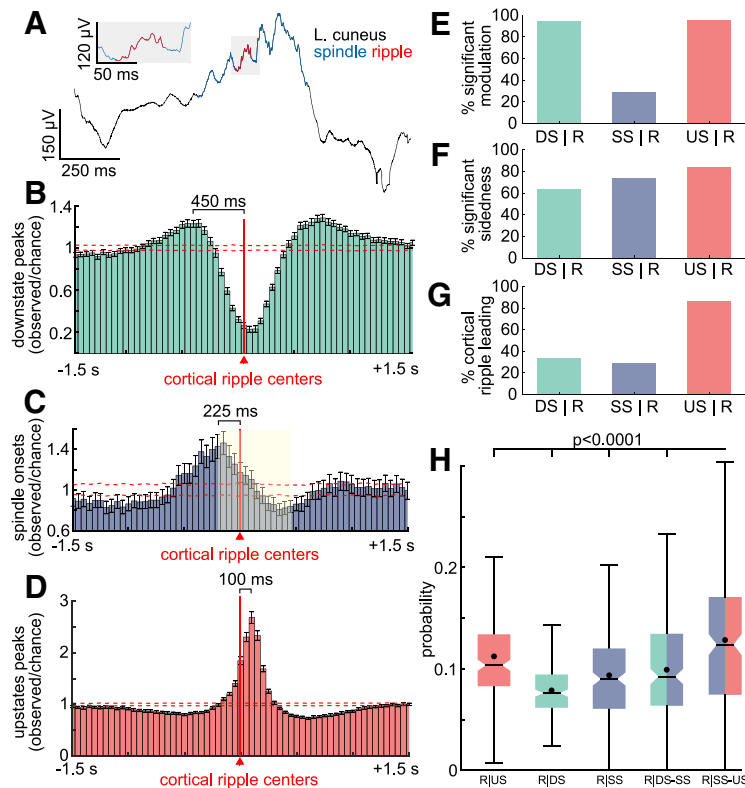


**Figure 10.** Cortical ripples occur during sleep spindles on the down-to-upstate transition during NREM. **A**, Example cortical ripple occurring during a spindle on a down-to-upstate transition during NREM. **B**, Times of downstate peaks plotted relative to local cortical ripple centers at  $t = 0$  across significant channels ( $N = 258/273$ , Patients S1–S17) during NREM. Downstate maxima occurred on average 450 ms before the cortical ripple center. Dashed red lines indicate 99% CI of the null distribution (200 shuffles/channel). **C**, Same as in **B**, but with spindle onsets ( $N = 80/273$ ). Spindles began on average 225 ms before the cortical ripple center, indicating that ripples occurred during spindles (yellow shaded area represents average spindle interval of 634 ms). **D**, Same as in **B**, but with upstate peaks ( $N = 260/273$ ). Upstate maxima occurred on average 100 ms after the cortical ripple center. **E**, Percent of channels with significant peri-ripple modulations of sleep waves detected on the same channels within  $\pm 1000$  ms (e.g., US | R represents upstate peaks relative to cortical ripples at  $t = 0$ ; one-sided randomization test, 200 shuffles, 50 ms nonoverlapping bins, 2 consecutive bins with post-FDR  $p < 0.05$  required for significance). DS and US were significantly associated with ripples in  $\sim 95\%$  of channels, sleep spindles less frequently. **F**, Percent of channels with significant modulations that had significant sidedness preference around  $t = 0$  (post-FDR  $p < 0.05$ , one-sided binomial test,  $-1000$  to  $-1$  ms vs  $1$ – $1000$  ms, expected = 0.5). **G**, Percent of channels with significant sidedness preference that had cortical ripples leading the other sleep waves (according to counts in  $-1000$  to  $-1$  ms vs  $1$ – $1000$  ms). Downstate peaks and spindle onsets typically preceded ripples, and upstate peaks followed. **H**, Probabilities of ripple centers preceding upstates, following downstates, occurring during spindles in isolation or during spindles following downstates (DS–SS), or during spindles preceding upstates (SS–US). The time window used following a downstate or preceding an upstate was 634 ms, which was the average spindle duration. The probability of a ripple occurring was greatest during spindles preceding upstates (post-FDR  $p < 0.0001$ , two-sided paired  $t$  test, channel-wise). Table 4 contains results from **E–G** in tabular format. DS, Downstate; SS, sleep spindle; US, upstate.

**Table 4. Sleep wave–ripple coupling<sup>a</sup>**

Graphoelement   ripple	Significant modulation	Significant sidedness	Cort-R leading
Downstate   Cort-R	94.51% (258/273)	63.57% (164/258)	33.54% (56/164)
Spindle   Cort-R	29.3% (80/273)	73.75% (59/80)	28.81% (17/59)
Upstate   Cort-R	95.24% (260/273)	83.85% (218/260)	86.70% (189/218)

<sup>a</sup>Proportion of channels with significant peri-ripple modulations of sleep waves detected on the same channels within  $\pm 1000$  ms (e.g., Upstate | Cort-R represents upstate peaks relative to cortical ripples at  $t = 0$ ; one-sided randomization test, 200 shuffles, 50 ms nonoverlapping bins, 2 consecutive bins with  $p < 0.05$  required for significance), and those with significant modulations that had significant sidedness preference around  $t = 0$  ( $p < 0.05$ , one-sided binomial test,  $-1000$  to  $-1$  ms vs  $1$ – $1000$  ms, expected = 0.5), and those with significant sidedness preference that had cortical ripples leading sleep waves (according to counts in  $-1000$  to  $-1$  ms vs  $1$ – $1000$  ms). In the calculations, upstate and downstate times were peaks and spindle times were onsets.  $p$  values were FDR-corrected across channels and bins. For single sweep example, see Figure 10A. For peri-ripple time histograms of cortical sleep waves, see Figure 10B–D. For graphical representations of conditional probabilities, see Figure 10E–G.

organization of cofiring by the phase of individual ripple cycles, we constructed a control dataset consisting of the neuronal firing during ripples where the spike times were randomly shuffled. Compared with this shuffled control, there was a significant increase in short-latency cofiring during ripples with their actual spike times (PY–PY: 1.21-fold increase,  $p = 1 \times 10^{-7}$ ,  $N = 4638$ ,  $t = 5.2$ ; PY–IN: 1.15-fold increase,  $p = 1 \times 10^{-7}$ ,  $N = 1561$ ,  $t = 5.2$ , one-sided paired  $t$  test). This finding indicates that the increase in cofiring is because of a specific organization of cofiring by the phase of the individual ripple cycles. Thus, ripples create a necessary and sufficient condition for STDP, and therefore may underlie the crucial contribution of these nested waves to consolidation (Dickey et al., 2021).

## Discussion

The current study provides the first comprehensive characterization of cortical ripples during waking and NREM in humans. Using intracranial recordings, we report that human cortical ripples are widespread during NREM in addition to waking. Basic ripple characteristics (occurrence rate, amplitude, oscillation frequency, duration, distribution across cortical areas) are stereotyped across electrodes and cortical parcels. They are also very similar in cortex versus hippocampus, and in NREM versus waking. Cortical ripple stereotypy and ubiquity across structures and states suggest that they may constitute a distinct and functionally important neurophysiological entity.

The characteristics of human ripples are similar to those of rodents with two exceptions. First, the center frequency of human ripples is focally  $\sim 90$  Hz (Jiang et al., 2019a), whereas in rodents it is  $\sim 130$  Hz (Khodagholy et al., 2017). Conceivably, the larger human brain may require more time for corticocortical and hippocampo-cortical integration than the rodent brain. The second apparent difference between humans and rodents is in cortical distribution. A previous rodent study found that cortical

ripples were restricted to association cortex (Khodagholy et al., 2017), and consistent observations were reported in humans (Vaz et al., 2019). In contrast, we recorded cortical ripples in all areas sampled, with slightly lower occurrence rates in association areas as indicated by the positive correlation between occurrence rate and myelination index.

In contrast to the similarities of basic properties, we found that ripples in waking versus NREM occur within much different immediate physiological contexts. In NREM, cortical ripples are strongly associated with local downstates and upstates, and less strongly with sleep spindles. Characteristically, ripples occur on the upslope  $\sim 100$  ms before the peak of the upstate. Previous studies found that sleep spindles (Dickey et al., 2021)

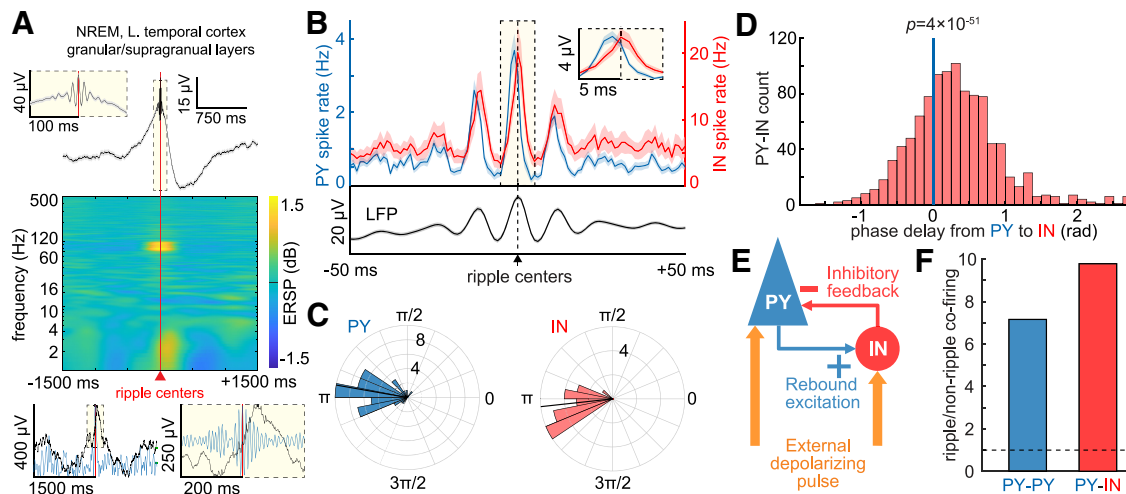


**Figure 11.** Pyramidal leads interneuronal cell firing at cortical ripple peaks. **A**, Superior temporal gyrus granular/supragranular layer ripples detected during NREM in a Utah Array recording. Top, Average broadband LFP. Middle, Average time-frequency. Bottom, Single-trial example trace in broadband LFP (black) and 70–100 Hz bandpass (blue, left represents analytic amplitude; right represents sweep). **B**, Mean broadband LFP locked to cortical ripple centers (black) and associated local PY (blue;  $N = 69$ ) and IN (red;  $N = 23$ ) spike rates during NREM. **C**, Circular mean 70–100 Hz phase of spikes of each PY ( $N = 47$ , mean = 2.97 rad,  $p = 5 \times 10^{-21}$ , Rayleigh test) and IN ( $N = 22$ , mean = 3.25 rad,  $p = 3 \times 10^{-13}$ ) during local cortical ripples (minimum 30 spikes per unit). PY spiking preceded IN spiking by 0.28 rad ( $p = 0.02$ , Watson–Williams test). The 0 rad corresponds to the trough, and  $\pi$  rad corresponds to the peak of the ripple. **D**, Circular mean ripple phase-lags of spikes from each PY ( $N = 47$ ) to each IN ( $N = 22$ ) ( $N = 1034$  unit pairs, mean =  $0.31 \pm 0.63$  rad,  $p = 4 \times 10^{-51}$ , one-sided one-sample  $t$  test). **E**, Pyramidal Interneuron Network Gamma ripple generation mechanism consistent with single-unit recordings, animal studies (Stark et al., 2014), and modeling (Buzsáki and Wang, 2012). Abrupt depolarization causes synchronous PY and IN firing, which then spike rhythmically, separated by fixed intervals because of recurrent inhibition. **F**, Pairs of PYs (PY–PY) cofire  $\sim 7$  times more often within 5 ms of each other during ripples compared with randomly selected epochs in between ripples matched in number and duration to the ripples. Similarly, PY–IN pairs cofire  $\sim 10$  times more during ripples. IN, Putative interneuron unit; PY, putative pyramidal unit.

and upstates (Csicsvari et al., 2010) are associated with strong increases in local unit firing, and we found that also to be the case for cortical ripples during NREM. Hippocampal ripples during NREM in previous studies were also found often to occur during local sharp-waves or spindles (Staresina et al., 2015; Jiang et al., 2019a,b,c).

Since sleep spindles and down-to-upstates are characteristic of NREM, they would not be expected to occur with waking ripples. Although we found no other lower-frequency wave to be consistently associated with ripples during waking, both cortical and hippocampal ripples occurred during greatly increased local  $>200$  Hz amplitude activity, a surrogate for unit firing (Mukamel et al., 2005). Thus, the local contexts of both cortical and hippocampal ripples, in both NREM and waking, are sudden increases in local excitability lasting at least as long as the ripple ( $\sim 70$  ms). NREM and waking are different in that the depolarizing pulse is organized by endogenous sleep rhythms in NREM, but appears to be related to exogenous input, such as a retrieval cue, during waking.

Computational neural models and experimental studies have found that depolarizing pulses can induce oscillations from  $\sim 20$  to 160 Hz (Buzsáki and Wang, 2012; Buzsáki, 2015). Depolarization causes synchronous PY firing, which is inhibited for a fixed time by recurrent inhibition from local basket cells. The PYs then fire again, resulting in Pyramidal Interneuron Network Gamma. As predicted by this model, we found strong ripple phase-modulation of putative PY and interneuronal firing, with PYs regularly preceding INs. Our findings are also consistent with Pyramidal Interneuron Network Gamma supplemented by synchronized basket cell firing and mutual inhibition (Interneuron Network Gamma) (Bartos et al., 2002). Definitive mechanistic demonstration would require experiments not currently possible *in vivo* in humans (Stark et al., 2014).

Previous studies have shown that cortical ripples occur on upstate and spindle peaks in cats (Grenier et al., 2001) and rats

(Khodagholy et al., 2017), and parahippocampal  $\gamma$  bursts of various frequencies occur on upstates in humans (Le Van Quyen et al., 2010). Here we report similar relationships in humans, consistent with a previous finding that cortical ripples during human NREM are suppressed during and increased following downstates (von Ellenrieder et al., 2016). The critical role of rodent hippocampal ripples in memory consolidation during NREM (Girardeau et al., 2009) is dependent on their association with cortical sleep waves (spindles, downstates, upstates) (Siapas and Wilson, 1998; Maingret et al., 2016; Latchoumane et al., 2017). In humans, hippocampal ripples are also associated with sleep waves (Staresina et al., 2015; Latchoumane et al., 2017; Jiang et al., 2019a,b), and cortical sleep waves are also associated with consolidation (Niknazar et al., 2015). Thus, our observation that human cortical ripples during NREM are strongly associated with upstates, and less strongly with downstates and spindles, is consistent with a role of human cortical ripples in consolidation. This is supported by a recent study showing that cortical ripples during NREM mark the replay of learned motor patterns from prior waking (Rubin et al., 2022).

Consolidation requires plasticity to increase the strength of the connections embodying the memory, which may occur when presynaptic and postsynaptic cells fire in close temporal proximity, termed STDP (Feldman, 2012). We show here that local neurons are much more likely to fire at delays optimal for STDP during ripples than control periods, and that cofiring is organized beyond what would be expected by a general increase in neuron firing. A similar increase is also observed during sleep spindles and upstates in humans (Dickey et al., 2021). Since we also show that NREM cortical ripples are temporally coordinated with sleep spindles and upstates, this supports a synergistic facilitation of plasticity. Thus, multiple characteristics of cortical ripples are consistent with them playing a role in consolidation, but direct confirmation of this role will require interventions that were not performed in the current study.

Recently, human waking cortical ripples were shown to mark spatiotemporal firing patterns during cued recall of items that reproduced those previously evoked by the same items during their initial presentation (Jiang et al., 2017). This suggests the possibility that ripples, in humans and rodents, NREM and waking, hippocampus and cortex, share a common role in contributing to the reconstruction of previously occurring firing patterns. The similar characteristics of human ripples, in NREM and waking, hippocampus and cortex, is consistent with this speculation.

Previous reports in rodents (Khodagholy et al., 2017) and humans (Vaz et al., 2019) that cortical ripples were restricted to association cortex were also interpreted as consistent with a selective interaction of cortical ripples with the hippocampus. However, in our more extensive sample of cortical sites, we observed a lower ripple density in higher associative cortex. Furthermore, we found no relationship across cortical parcels between their degree of connectivity with the hippocampal formation (inferred from diffusion imaging) (Rosen and Halgren, 2021) and cortical ripple density or any other ripple characteristic. Indeed, in other work, we have shown that cortical ripples are more likely to co-occur and phase-lock with other cortical sites than the hippocampus (Dickey et al., 2022). Thus, the functional role of cortical ripples may not be confined to memory consolidation and recall.

In conclusion, the current study provides the first report of cortical ripples during sleep in humans. Cortical ripples during NREM were found to have basic characteristics (duration, oscillation frequency, and occurrence rate) that are highly similar to those of cortical ripples during waking as well as hippocampal ripples. Cortical ripple oscillation frequencies were tightly focused at  $\sim 90$  Hz. This finding, together with their stereotypy and ubiquity across structures and states, suggests that cortical ripples may constitute a distinct and functionally important neurophysiological entity. Unit firing during human cortical NREM ripples supported the mechanism proposed for rodent hippocampal ripples, based on PY-IN feedback. Cortical ripples during NREM characteristically occurred after downstates, during spindles, shortly before the peak of the upstate, an association and timing that are important for the consolidation of memories during sleep. Furthermore, NREM cortical ripples were associated with increased local cofiring between units, thus fulfilling a fundamental requirement for STDP. However, cortical ripples were widespread across cortical parcels, regardless of their probable connectivity with the hippocampus. Overall, these characteristics of cortical ripples during human NREM are consistent with a role that includes but may not be limited to sleep-dependent memory consolidation.

## References

- Axmacher N, Elger CE, Fell J (2008) Ripples in the medial temporal lobe are relevant for human memory consolidation. *Brain* 131:1806–1817.
- Bartos M, Vida I, Frotscher M, Meyer A, Monyer H, Geiger JR, Jonas P (2002) Fast synaptic inhibition promotes synchronized gamma oscillations in hippocampal interneuron networks. *Proc Natl Acad Sci USA* 99:13222–13227.
- Bazhenov M, Rulkov NF, Timofeev I (2008) Effect of synaptic connectivity on long-range synchronization of fast cortical oscillations. *J Neurophysiol* 100:1562–1575.
- Bechtold B (2016) Violin plots for Matlab. Github Project.
- Behrens TE, Berg HJ, Jbabdi S, Rushworth MF, Woolrich MW (2007) Probabilistic diffusion tractography with multiple fibre orientations: what can we gain? *Neuroimage* 34:144–155.
- Benjamini Y, Hochberg Y (1995) Controlling the false discovery rate: a practical and powerful approach to multiple testing. *J R Stat Soc B* 57:289–300.
- Berens P (2009) CircStat: a MATLAB toolbox for circular statistics. *J Stat Softw* 31:1–21.
- Bragin A, Engel J Jr, Wilson CL, Fried I, Buzsáki G (1999) High-frequency oscillations in human brain. *Hippocampus* 9:137–142.
- Buzsáki G (2015) Hippocampal sharp wave-ripple: a cognitive biomarker for episodic memory and planning. *Hippocampus* 25:1073–1188.
- Buzsáki G, Wang XJ (2012) Mechanisms of gamma oscillations. *Annu Rev Neurosci* 35:203–225.
- Chan AM, Dykstra AR, Jayaram V, Leonard MK, Travis KE, Gygi B, Baker JM, Eskandar E, Hochberg LR, Halgren E, Cash SS (2014) Speech-specific tuning of neurons in human superior temporal gyrus. *Cereb Cortex* 24:2679–2693.
- Clemens Z, Molle M, Eross L, Barsi P, Halasz P, Born J (2007) Temporal coupling of parahippocampal ripples, sleep spindles and slow oscillations in humans. *Brain* 130:2868–2878.
- Csercsa R, et al. (2010) Laminar analysis of slow wave activity in humans. *Brain* 133:2814–2829.
- Dehghani N, Peyrache A, Telenczuk B, Le Van Quyen M, Halgren E, Cash SS, Hatsopoulos NG, Destexhe A (2016) Dynamic balance of excitation and inhibition in human and monkey neocortex. *Sci Rep* 6:23176.
- Delorme A, Makeig S (2004) EEGLAB: an open source toolbox for analysis of single-trial EEG dynamics including independent component analysis. *J Neurosci Methods* 134:9–21.
- Desikan RS, Segonne F, Fischl B, Quinn BT, Dickerson BC, Blacker D, Buckner RL, Dale AM, Maguire RP, Hyman BT, Albert MS, Killiany RJ (2006) An automated labeling system for subdividing the human cerebral cortex on MRI scans into gyral based regions of interest. *Neuroimage* 31:968–980.
- Destrieux C, Fischl B, Dale A, Halgren E (2010) Automatic parcellation of human cortical gyri and sulci using standard anatomical nomenclature. *Neuroimage* 53:1–15.
- Dickey CW, Sargsyan A, Madsen JR, Eskandar EN, Cash SS, Halgren E (2021) Travelling spindles create necessary conditions for spike timing-dependent plasticity in humans. *Nat Commun* 12:1027.
- Dickey CW, Verzhbivsky IA, Jiang X, Rosen BQ, Kajfez S, Stedelin B, Shih JJ, Ben-Haim S, Raslan AM, Eskandar EN, Gonzalez-Martinez J, Cash SS, Halgren E (2022) Widespread ripples synchronize human cortical activity during sleep, waking, and memory recall. *Proc Natl Acad Sci USA* 119: e2107797119.
- Ego-Stengel V, Wilson MA (2010) Disruption of ripple-associated hippocampal activity during rest impairs spatial learning in the rat. *Hippocampus* 20:1–10.
- Eichenlaub JB, Jarosiewicz B, Saab J, Franco B, Kelemen J, Halgren E, Hochberg LR, Cash SS (2020) Replay of learned neural firing sequences during rest in human motor cortex. *Cell Rep* 31:107581.
- Fedorov A, Beichel R, Kalpathy-Cramer J, Finet J, Fillion-Robin JC, Pujol S, Bauer C, Jennings D, Fennessy F, Sonka M, Buatti J, Aylward S, Miller JV, Pieper S, Kikinis R (2012) 3D Slicer as an image computing platform for the Quantitative Imaging Network. *Magn Reson Imaging* 30:1323–1341.
- Feldman DE (2012) The spike-timing dependence of plasticity. *Neuron* 75:556–571.
- Fernández E, Greger B, House PA, Aranda I, Botella C, Albusua J, Soto-Sánchez C, Alfaro A, Normann RA (2014) Acute human brain responses to intracortical microelectrode arrays: challenges and future prospects. *Front Neuroeng* 7:24.
- Fischl B (2012) FreeSurfer. *Neuroimage* 62:774–781.
- Fischl B, Sereno MI, Tootell RB, Dale AM (1999) High-resolution intersubject averaging and a coordinate system for the cortical surface. *Hum Brain Mapp* 8:272–284.
- Fischl B, van der Kouwe A, Destrieux C, Halgren E, Ségonne F, Salat DH, Busa E, Seidman LJ, Goldstein J, Kennedy D, Caviness V, Makris N, Rosen B, Dale AM (2004) Automatically parcellating the human cerebral cortex. *Cereb Cortex* 14:11–22.
- Girardeau G, Benchenane K, Wiener SI, Buzsáki G, Zugaro MB (2009) Selective suppression of hippocampal ripples impairs spatial memory. *Nat Neurosci* 12:1222–1223.
- Glasser MF, Coalson TS, Robinson EC, Hacker CD, Harwell J, Yacoub E, Ugurbil K, Andersson J, Beckmann CF, Jenkinson M, Smith SM, Van Essen DC (2016) A multi-modal parcellation of human cerebral cortex. *Nature* 536:171–178.

- Gonzalez CE, Mak-McCully RA, Rosen BQ, Cash SS, Chauvel PY, Bastuji H, Rey M, Halgren E (2018) Theta bursts precede, and spindles follow, cortical and thalamic downstates in human NREM sleep. *J Neurosci* 38:9989–10001.
- Grenier F, Timofeev I, Steriade M (2001) Focal synchronization of ripples (80–200 Hz) in neocortex and their neuronal correlates. *J Neurophysiol* 86:1884–1898.
- Hagler DJ Jr, Ulbert I, Wittner L, Erőss L, Madsen JR, Devinsky O, Doyle W, Fabó D, Cash SS, Halgren E (2018) Heterogeneous origins of human sleep spindles in different cortical layers. *J Neurosci* 38:3013–3025.
- Iglesias JE, Augustinack JC, Nguyen K, Player CM, Player A, Wright M, Roy N, Frosch MP, McKee AC, Wald LL, Fischl B, Van Leemput K, Alzheimer's Disease Neuroimaging Initiative. (2015) A computational atlas of the hippocampal formation using ex vivo, ultra-high resolution MRI: application to adaptive segmentation of in vivo MRI. *Neuroimage* 115:117–137.
- Ji D, Wilson MA (2007) Coordinated memory replay in the visual cortex and hippocampus during sleep. *Nat Neurosci* 10:100–107.
- Jiang X, Shamie I, Doyle WK, Friedman D, Dugan P, Devinsky O, Eskandar E, Cash SS, Thesen T, Halgren E (2017) Replay of large-scale spatio-temporal patterns from waking during subsequent NREM sleep in human cortex. *Sci Rep* 7:17380.
- Jiang X, Gonzalez-Martinez J, Halgren E (2019a) Coordination of human hippocampal sharpwave ripples during NREM sleep with cortical theta bursts, spindles, downstates, and upstates. *J Neurosci* 39:8744–8761.
- Jiang X, Gonzalez-Martinez J, Halgren E (2019b) Posterior hippocampal spindle-ripples co-occur with neocortical theta-bursts and downstates, and phase-lock with parietal spindles during NREM sleep in humans. *J Neurosci* 39:8949–8968.
- Jiang X, Gonzalez-Martinez J, Cash SS, Chauvel P, Gale J, Halgren E (2019c) Improved identification and differentiation from epileptiform activity of human hippocampal sharp wave ripples during NREM sleep. *Hippocampus* 30:610–622.
- Johnson H, Harris G, Williams K (2007) BRAINSFIT: Mutual information registrations of whole-brain 3D Images, using the insight toolkit.
- Johnson LA, Euston DR, Tatsuno M, McNaughton BL (2010) Stored-trace reactivation in rat prefrontal cortex is correlated with down-to-up state fluctuation density. *J Neurosci* 30:2650–2661.
- Kamiński J, Brzezicka A, Mamelak AN, Rutishauser U (2020) Combined phase-rate coding by persistently active neurons as a mechanism for maintaining multiple items in working memory in humans. *Neuron* 106:256–264.e253.
- Keller CJ, Truccolo W, Gale JT, Eskandar E, Thesen T, Carlson C, Devinsky O, Kuzniecky R, Doyle WK, Madsen JR, Schomer DL, Mehta AD, Brown EN, Hochberg LR, Ulbert I, Halgren E, Cash SS (2010) Heterogeneous neuronal firing patterns during interictal epileptiform discharges in the human cortex. *Brain* 133:1668–1681.
- Khodagholy D, Gelineas JN, Buzsáki G (2017) Learning-enhanced coupling between ripple oscillations in association cortices and hippocampus. *Science* 358:369–372.
- Latchoumane CF, Ngo HV, Born J, Shin HS (2017) Thalamic spindles promote memory formation during sleep through triple phase-locking of cortical, thalamic, and hippocampal rhythms. *Neuron* 95:424–435.e426.
- Le Van Quyen M, Bragin A, Staba R, Crépon B, Wilson CL, Engel J (2008) Cell type-specific firing during ripple oscillations in the hippocampal formation of humans. *J Neurosci* 28:6104–6110.
- Le Van Quyen M, Staba R, Bragin A, Dickson C, Valderrama M, Fried I, Engel J (2010) Large-scale microelectrode recordings of high-frequency gamma oscillations in human cortex during sleep. *J Neurosci* 30:7770–7782.
- Le Van Quyen M, Muller LE, Teleniczuk B, Halgren E, Cash S, Hatsopoulos NG, Dehghani N, Destexhe A (2016) High-frequency oscillations in human and monkey neocortex during the wake-sleep cycle. *Proc Natl Acad Sci USA* 113:9363–9368.
- Maingret N, Girardeau G, Todorova R, Goutierre M, Zugaro M (2016) Hippocampo-cortical coupling mediates memory consolidation during sleep. *Nat Neurosci* 19:959–964.
- Mak-McCully RA, Rosen BQ, Rolland M, Régis J, Bartolomei F, Rey M, Chauvel P, Cash SS, Halgren E (2015) Distribution, amplitude, incidence, co-occurrence, and propagation of human K-complexes in focal transcorical recordings. *eNeuro* 2:ENEURO.0028-15.2015.
- Mukamel R, Gelbard H, Arieli A, Hasson U, Fried I, Malach R (2005) Coupling between neuronal firing, field potentials, and fMRI in human auditory cortex. *Science* 309:951–954.
- Niknazar M, Krishnan GP, Bazhenov M, Mednick SC (2015) Coupling of thalamocortical sleep oscillations are important for memory consolidation in humans. *PLoS One* 10:e0144720.
- Norman Y, Yeagle EM, Khuvis S, Harel M, Mehta AD, Malach R (2019) Hippocampal sharp-wave ripples linked to visual episodic recollection in humans. *Science* 365:eaax1030.
- Oostenveld R, Fries P, Maris E, Schoffelen JM (2011) FieldTrip: open source software for advanced analysis of MEG, EEG, and invasive electrophysiological data. *Comput Intell Neurosci* 2011:156869.
- Pesaran B, Pezaris JS, Sahani M, Mitra PP, Andersen RA (2002) Temporal structure in neuronal activity during working memory in macaque parietal cortex. *Nat Neurosci* 5:805–811.
- Peyrache A, Khamassi M, Benchenane K, Wiener SI, Battaglia FP (2009) Replay of rule-learning related neural patterns in the prefrontal cortex during sleep. *Nat Neurosci* 12:919–926.
- Peyrache A, Dehghani N, Eskandar EN, Madsen JR, Anderson WS, Donoghue JA, Hochberg LR, Halgren E, Cash SS, Destexhe A (2012) Spatiotemporal dynamics of neocortical excitation and inhibition during human sleep. *Proc Natl Acad Sci USA* 109:1731–1736.
- Pouzat C, Mazor O, Laurent G (2002) Using noise signature to optimize spike-sorting and to assess neuronal classification quality. *J Neurosci Methods* 122:43–57.
- Ray S (2015) Challenges in the quantification and interpretation of spike-LFP relationships. *Curr Opin Neurobiol* 31:111–118.
- Rosen BQ, Halgren E (2021) A whole-cortex probabilistic diffusion tractography connectome. *eNeuro* 8:ENEURO.0416-20.2020.
- Rubin DB, Hosman T, Kelemen JN, Kapitovava A, Willett FR, Coughlin BF, Halgren E, Kimchi EY, Williams ZM, Simeral JD, Hochberg LR, Cash SS (2022) Learned motor patterns are replayed in human motor cortex during sleep. *J Neurosci* 42:5007–5020.
- Siapas AG, Wilson MA (1998) Coordinated interactions between hippocampal ripples and cortical spindles during slow-wave sleep. *Neuron* 21:1123–1128.
- Staba RJ, Wilson CL, Bragin A, Jhung D, Fried I, Engel J (2004) High-frequency oscillations recorded in human medial temporal lobe during sleep. *Ann Neurol* 56:108–115.
- Staresina BP, Bergmann TO, Bonnefond M, van der Meij R, Jensen O, Deuker L, Elger CE, Axmacher N, Fell J (2015) Hierarchical nesting of slow oscillations, spindles and ripples in the human hippocampus during sleep. *Nat Neurosci* 18:1679–1686.
- Stark E, Roux L, Eichler R, Senzai Y, Royer S, Buzsáki G (2014) Pyramidal cell-interneuron interactions underlie hippocampal ripple oscillations. *Neuron* 83:467–480.
- Steiger JH (1980) Tests for comparing elements of a correlation matrix. *Psychol Bull* 87:245–251.
- Teleniczuk B, Dehghani N, Le Van Quyen M, Cash SS, Halgren E, Hatsopoulos NG, Destexhe A (2017) Local field potentials primarily reflect inhibitory neuron activity in human and monkey cortex. *Sci Rep* 7:40211.
- Vaz AP, Inati SK, Brunel N, Zaghoul KA (2019) Coupled ripple oscillations between the medial temporal lobe and neocortex retrieve human memory. *Science* 363:975–978.
- Vaz AP, Wittig JH, Inati SK, Zaghoul KA (2020) Replay of cortical spiking sequences during human memory retrieval. *Science* 367:1131–1134.
- von Ellenrieder N, Frauscher B, Dubeau F, Gotman J (2016) Interaction with slow waves during sleep improves discrimination of physiologic and pathologic high-frequency oscillations (80–500 Hz). *Epilepsia* 57:869–878.
- Waziri A, Schevon CA, Cappell J, Emerson RG, McKhann GM 2nd, Goodman RR (2009) Initial surgical experience with a dense cortical microarray in epileptic patients undergoing craniotomy for subdural electrode implantation. *Neurosurgery* 64:540–545; discussion 545.
- Wilson MA, McNaughton BL (1994) Reactivation of hippocampal ensemble memories during sleep. *Science* 265:676–679.